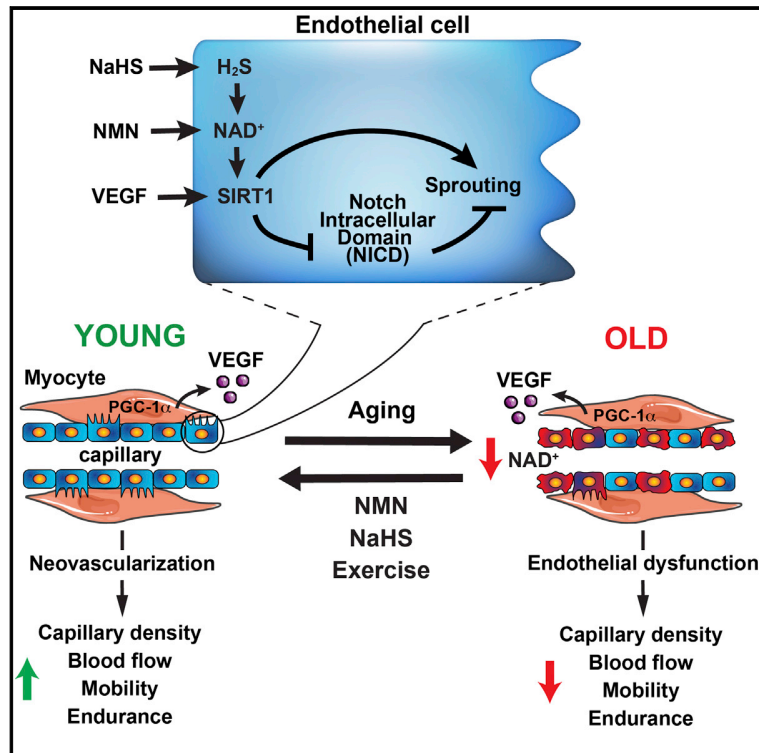


Impairment of an Endothelial NAD⁺-H₂S Signaling Network Is a Reversible Cause of Vascular Aging

Graphical Abstract



Authors

Abhirup Das, George X. Huang, Michael S. Bonkowski, ..., Zolt Arany, Leonard Guarente, David A. Sinclair

Correspondence

zarany@mail.med.upenn.edu (Z.A.), leng@mit.edu (L.G.), david_sinclair@hms.harvard.edu (D.A.S.)

In Brief

Endothelial SIRT1 regulates pro-angiogenic signals secreted from myocytes and improves muscle health. Treatment of mice with NAD⁺ precursor nicotinamide mononucleotide improves vascular and increases endurance in aging mice.

Highlights

- Reduced blood flow with age is due to loss of endothelial NAD⁺-SIRT1 activity
- NAD⁺ and H₂S control muscle angiogenesis and increase endurance in old mice
- The NAD precursor NMN mimics and augments exercise by inhibiting NICD-Notch
- Neovascularization is as important as mitochondria for rejuvenating muscle

Impairment of an Endothelial NAD⁺-H₂S Signaling Network Is a Reversible Cause of Vascular Aging

Abhirup Das,^{1,2,3,8} George X. Huang,^{1,4,8} Michael S. Bonkowski,¹ Alban Longchamp,⁵ Catherine Li,² Michael B. Schultz,¹ Lynn-Jee Kim,² Brenna Osborne,⁶ Sanket Joshi,⁶ Yuancheng Lu,¹ Jose Humberto Treviño-Villarreal,⁵ Myung-Jin Kang,² Tzong-tyng Hung,⁷ Brendan Lee,⁷ Eric O. Williams,³ Masaki Igarashi,³ James R. Mitchell,⁵ Lindsay E. Wu,² Nigel Turner,⁶ Zolt Arany,^{4,*} Leonard Guarente,^{3,*} and David A. Sinclair^{1,2,9,*}

¹Paul F. Glenn Center for the Biological Mechanisms of Aging, Department of Genetics, Harvard Medical School, Boston, MA 02115, USA

²Laboratory for Ageing Research, Department of Pharmacology, School of Medical Sciences, The University of New South Wales, Sydney, NSW 2052, Australia

³Paul F. Glenn Center for Science of Aging Research, Department of Biology, Massachusetts Institute of Technology, Cambridge, MA 02139, USA

⁴Cardiovascular Institute, Perelman School of Medicine, University of Pennsylvania, 3400 Civic Center Boulevard, Bldg. 421, Philadelphia, PA 19104, USA

⁵Department of Genetics and Complex Diseases, Harvard T.H. Chan School of Public Health, Boston, MA, USA

⁶Mitochondrial Bioenergetics Laboratory, Department of Pharmacology, School of Medical Sciences, The University of New South Wales, Sydney, NSW 2052, Australia

⁷Biological Resources Imaging Laboratory, Mark Wainwright Analytical Centre, The University of New South Wales, Sydney, NSW 2052, Australia

⁸Senior author

⁹Lead Contact

*Correspondence: zarany@mail.med.upenn.edu (Z.A.), leng@mit.edu (L.G.), david_sinclair@hms.harvard.edu (D.A.S.)
<https://doi.org/10.1016/j.cell.2018.02.008>

SUMMARY

A decline in capillary density and blood flow with age is a major cause of mortality and morbidity. Understanding why this occurs is key to future gains in human health. NAD⁺ precursors reverse aspects of aging, in part, by activating sirtuin deacylases (SIRT1–SIRT7) that mediate the benefits of exercise and dietary restriction (DR). We show that SIRT1 in endothelial cells is a key mediator of pro-angiogenic signals secreted from myocytes. Treatment of mice with the NAD⁺ precursor nicotinamide mononucleotide (NMN) improves blood flow and increases endurance in elderly mice by promoting SIRT1-dependent increases in capillary density, an effect augmented by exercise or increasing the levels of hydrogen sulfide (H₂S), a DR mimetic and regulator of endothelial NAD⁺ levels. These findings have implications for improving blood flow to organs and tissues, increasing human performance, and reestablishing a virtuous cycle of mobility in the elderly.

INTRODUCTION

One of the most profound changes to the body as it ages is a decline in the number and function of endothelial cells (ECs) that line the vasculature. The performance of organs and tissues

is critically dependent on a functional microcapillary network that maintains a supply of oxygen, exchanges heat and nutrients, and removes waste products (Olfert et al., 2009). According to the Vascular Theory of Aging (Le Couteur and Lakatta, 2010), vascular decline is one of the major causes of aging and age-related diseases.

Despite the importance of capillary loss to human health, it is surprising how little we understand about its underlying causes (Le Couteur and Lakatta, 2010). Exercise is currently the best way to delay the effects of aging on the microvasculature by promoting neovascularization, but little is known about why tissues become desensitized to exercise with age (Bassel-Duby and Olson, 2006; Booth and Thomason, 1991; Hood, 2001). Skeletal muscle is an ideal tissue to study the effects of aging on neovascularization and capillary maintenance. For reasons that are unclear, as we age there is an increase in muscle EC apoptosis, decreased neovascularization, and blood vessel loss (Groen et al., 2014; Wang et al., 2014), resulting in reduced muscle mass (sarcopenia) and a decline in strength and endurance in the later decades of life, even with exercise (Denis et al., 1986; Prior et al., 2016; Ryan et al., 2006). A few exercise-mimetic agents have been reported that increase mitochondrial function (e.g., resveratrol and PPAR δ agonists), none of which are known to work by increasing capillary density or blood flow (Cantó et al., 2012; Lagouge et al., 2006; Narkar et al., 2008).

SIRT1 is a member of the sirtuin family of NAD⁺-dependent deacylases that mediate the health benefits of dietary restriction (DR) and can extend lifespan when overexpressed (Guarente, 2013; Haigis and Sinclair, 2010; Kanfi et al., 2012; Satoh et al.,

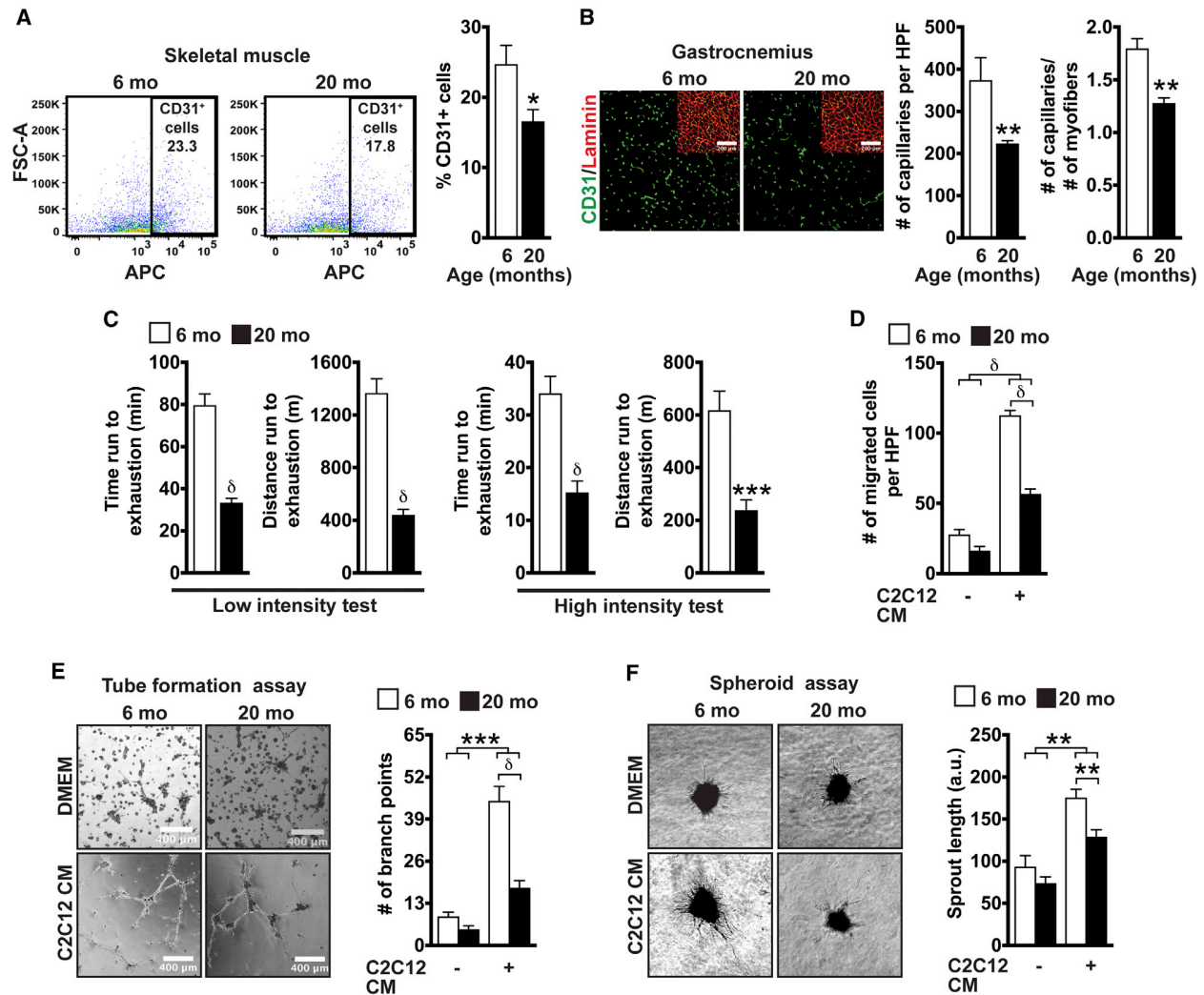


Figure 1. Aging Is Associated with Decreased Muscle Angiogenesis and Endurance

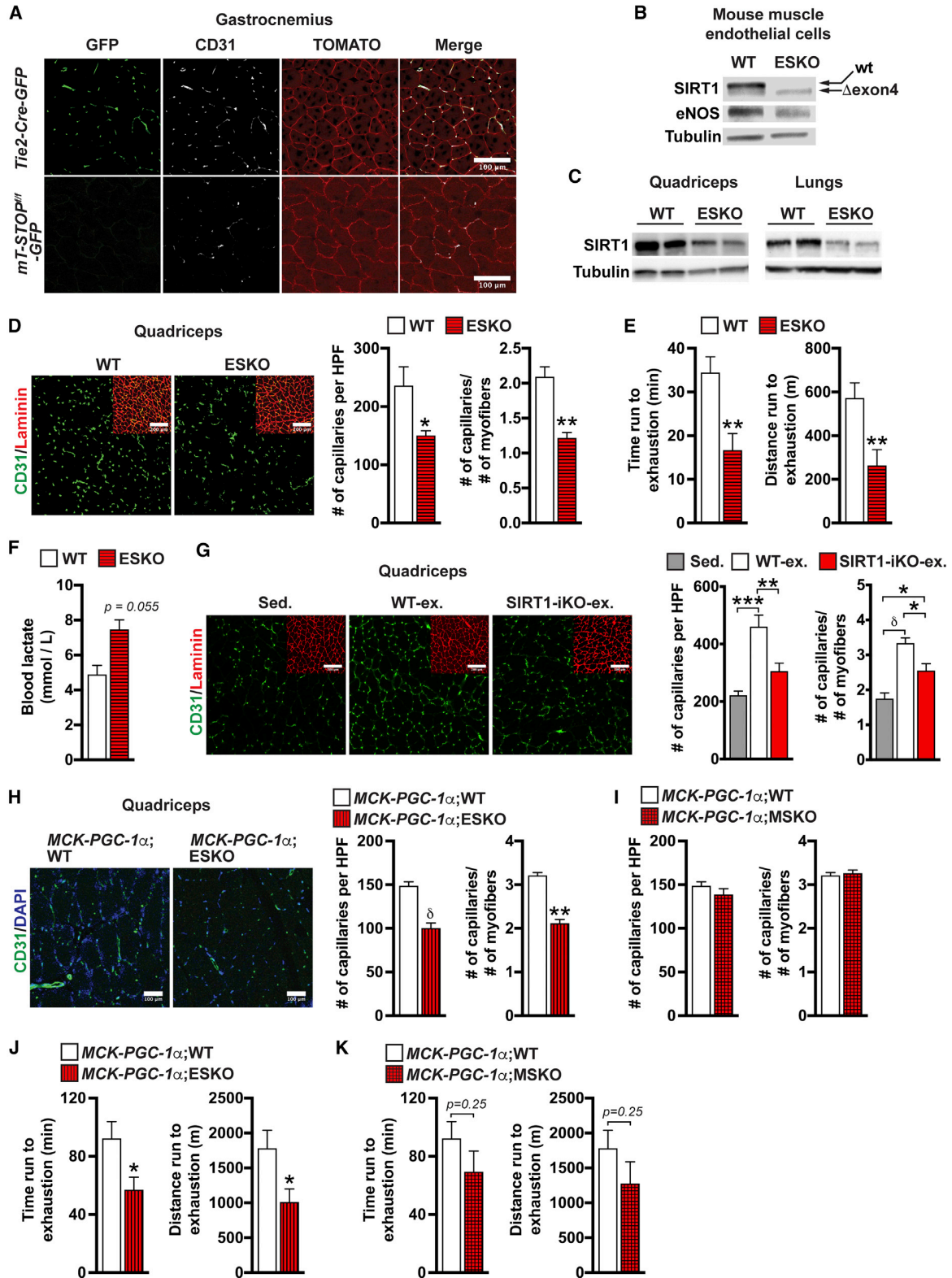
(A) Flow cytometry plots and percent CD31⁺ ECs in skeletal muscle of young and old mice (n = 7).
 (B) Gastrocnemius sections (20 \times) showing CD31 and laminin staining. Number of capillaries and capillary/fiber ratio per high power field (HPF) (n = 7).
 (C) Duration and distance run by mice until exhaustion (n = 11).
 (D) Number of migrated MLECs in a transwell (n = 10).
 (E) Images and number of branch points of tube networks formed by MLECs (n = 8).
 (F) Images and sprout length of MLEC spheroids (n = 10).

Data expressed as mean \pm SEM. *p < 0.05, **p < 0.005, ***p < 0.0005, δ p < 0.00005 by Student's t test (A–C) or two-way ANOVA with Bonferroni's correction (D–F). See also Figure S1.

2013). In young muscle, SIRT1 is required for ischemia-induced neovascularization (Potente et al., 2007), vascular relaxation (Mattagajasingh et al., 2007; Pearson et al., 2008; Ungvari et al., 2010), and is implicated in EC senescence (Ota et al., 2007; Zu et al., 2010). It is, however, unknown whether endothelial SIRT1 regulates microvascular remodeling in skeletal muscle tissue, and if so, whether its breakdown with age is cell-autonomous or reversible.

SIRT1-activating compounds (STACs) such as resveratrol and SRT1720 have been pursued as a strategy for ameliorating age-related diseases (Hubbard et al., 2013; Sinclair and Guarente,

2014). A more recent approach has been to restore NAD⁺ levels by treating with NAD⁺ precursors such as nicotinamide riboside (NR) or nicotinamide mononucleotide (NMN) (Cantó et al., 2015; Gomes et al., 2013; Mouchiroud et al., 2013; Ramsey et al., 2008). NAD⁺ precursors increase the angiogenic capacity of ECs in cell culture (Borradaile and Pickering, 2009; Hughes-Large et al., 2014), improve the exercise capacity of young mice (Cantó et al., 2012), and protect against age-related physiological decline including reduced DNA repair, mitochondrial dysfunction, and glucose intolerance (de Picciotto et al., 2016; Gomes et al., 2013; Li et al., 2017; Yoshino et al., 2011). Whether



(legend on next page)

a decrease in NAD⁺ and SIRT1 activity in ECs is a cause of microvasculature loss and frailty during aging is not yet known.

Another DR mimetic is hydrogen sulfide (H₂S), a gas generated endogenously by cystathionine β-synthase (CBS) and/or cystathionine γ-lyase (CSE) (Hine and Mitchell, 2015). Evidence indicates that SIRT1 and H₂S may lie in the same pathway. For example, in *Caenorhabditis elegans*, hydrogen sulfide (H₂S) extends lifespan in a Sir2.1-dependent manner (Miller and Roth, 2007). In mammals, ectopic treatment with H₂S induces SIRT1 in response to oxidative stress (Suo et al., 2013; Wu et al., 2015; Zheng et al., 2014) and protects rat hearts from ischemia/reperfusion via a mechanism requiring SIRT1 (Hu et al., 2016).

In this study, we tested whether a decline in SIRT1 activity in ECs is a major reason why blood flow and endurance decrease with age, and whether SIRT1 stimulation by NMN and/or H₂S can reverse these changes. We show that loss of endothelial SIRT1 results in an early decline in skeletal muscle vascular density and exercise capacity, while overexpression of endothelial SIRT1 has a protective effect, ostensibly by sensitizing ECs to vascular endothelial growth factor (VEGF) coming from muscle fibers. Pharmacologically raising NAD⁺ levels promotes muscle vascular remodeling following ischemic injury and restores capillary density and treadmill endurance of old mice back to youthful levels, and in young mice during chronic exercise, an effect that is further augmented by H₂S.

RESULTS

Aging Is Associated with Decreased Muscle Microvasculature, Endurance, and Angiogenesis

One of the most reliable, yet pernicious aspects of mammalian aging is a decrease in blood flow to skeletal muscle. Consistent with this, the abundance of ECs and capillaries in skeletal muscle and exercise endurance of 20-month-old mice was significantly lower compared to 6-month-olds (Figures 1A–1C and S1A).

A possible explanation was impaired angiogenic potential. To test this, a series of *in vitro* angiogenesis assays were performed on mouse lung ECs (MLECs) from young and old mice. MLECs were cultured in the presence of conditioned media (CM)

with angiogenic factors provided by peroxisome proliferator-activated receptor γ coactivator 1-α (PGC-1α)-overexpressing C2C12 myotubes (Arany et al., 2008). Compared to young mice, MLECs from 20-month-old mice had reduced migratory capacity (Figures 1D and S1B), decreased ability to form capillary-like structures (Figures 1E and S1C), and shorter spheroidal sprout lengths (Figure 1F).

Endothelial SIRT1 Deletion Mimics the Effect of Aging on Capillary Density and Endurance

To test if SIRT1 is required for vascular maintenance and angiogenesis late in life, we used a *Tie2-Cre* mouse to knock out or overexpress SIRT1 specifically in the ECs. The EC-specificity of *Tie2* promoter was confirmed using a GFP reporter mouse strain (Figures 2A and S2A–S2D). Endothelial-specific SIRT1 knockout mice (ESKO) (Figures 2B, 2C, S2E, and S2F) were healthy and born in expected Mendelian ratios. In 6-month-old ESKO mice, the density and number of capillaries was significantly lower compared to age-matched wild-type (WT) mice (Figures 2D and S2G).

Although there were no obvious physiological differences between the genotypes (Figures S2H–S2J), in a high intensity endurance test ESKO mice ran only half as long and far as their WT littermates (Figure 2E; Movie S1). There was also a trend toward higher post-exercise serum lactate levels in ESKO mice ($p = 0.055$) (Figure 2F).

Differences in exercise capacity are commonly attributable to changes in muscle fiber type (Pette and Staron, 2000) or mitochondrial content (Lin et al., 2002). A comparison of gastrocnemius and quadriceps muscles from ESKO and WT mice showed no significant differences in fiber type (Figure S2K), mitochondrial content (Figure S2L), or mitochondrial activity (Figure S2M), further supporting the hypothesis that the low exercise capacity of ESKO mice is due to a reduced number of capillaries.

Endothelial SIRT1 Is Required for Exercise-Induced Neovascularization

In young individuals, exercise is a potent stimulator of angiogenesis, but this effect wanes considerably with advancing age for reasons that are not known. To test if SIRT1 plays a role in this

Figure 2. Endothelial SIRT1 Deletion Mimics the Effect of Aging on Capillary Density and Endurance

(A) Gastrocnemius sections (40×) showing GFP, CD31 and mTOMATO protein expression.

(B) SIRT1 and eNOS protein abundance in ECs isolated from skeletal muscle of WT and ESKO mice. SIRT1 exon 4 excision in ESKO results in SIRT1 band (Δexon4) running slightly below the WT band. Tubulin serves as a loading control.

(C) SIRT1 protein in lung and quadriceps. Tubulin serves as a loading control.

(D) Quadriceps sections (20×) showing CD31 and laminin staining. Number of capillaries and capillary/fiber ratio (6-month-old, $n = 8$).

(E) Duration and distance run until exhaustion in a high intensity treadmill test (6-month-old, $n = 8$).

(F) Post-exercise serum lactate levels (6-month-old, $n = 5$).

(G) Quadriceps sections (20×) from sedentary (SIRT1-iKO + WT) and exercised mice showing CD31 and laminin staining. Number of capillaries and capillary/fiber ratio (10-month-old, $n = 6$).

(H) Quadriceps sections (40×) showing DAPI and CD31 staining. Number of capillaries and capillary/fiber ratio (4-month-old, $n = 6$).

(I) Number of capillaries and capillary/fiber ratio in the quadriceps (4-month-old, $n = 6$).

(J) Duration and distance run until exhaustion in high intensity treadmill test (4-month-old, $n = 7$).

(K) Duration and distance run until exhaustion in high intensity treadmill test (4-month-old, $n = 7$).

Data expressed as mean ± SEM. * $p < 0.05$, ** $p < 0.005$, *** $p < 0.0005$, ⁵ $p < 0.00005$ by Student's t test (D–F, H, J, and K) or one-way ANOVA with Bonferroni's corrections (G).

See also Figure S2 and Movie S1.

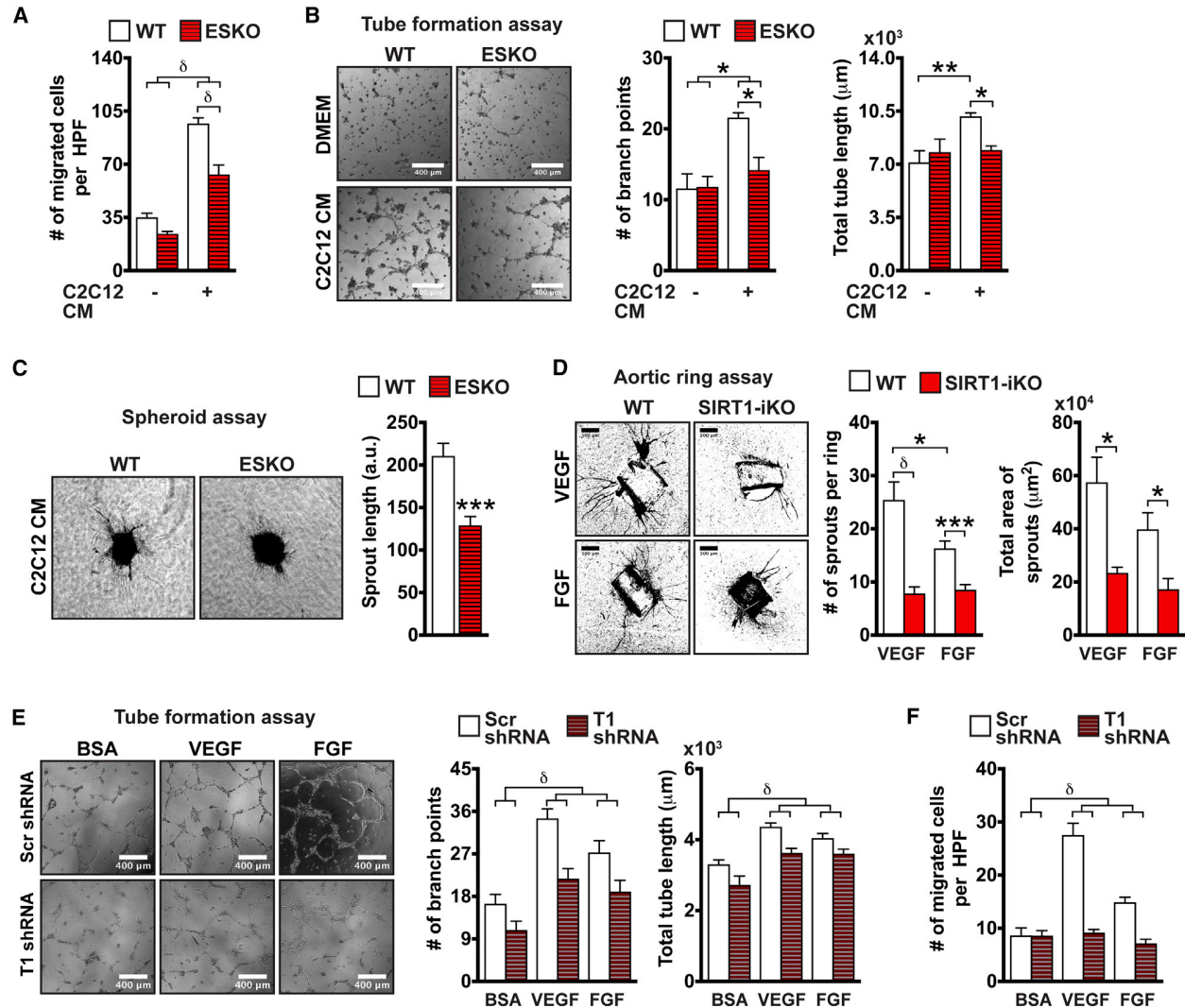


Figure 3. SIRT1 Is Required for Angiogenesis In Vitro

(A) Number of migrated MLECs (n = 12).

(B) Images, number of branch points, and length of tube networks formed by MLECs (n = 5).

(C) Images and sprout length of MLEC spheroids (n = 8).

(D) Images, number, and total area of microvessel sprouts in aortic rings (n = 8).

(E) Images, number of branch points, and length of tube networks formed by HAECs infected with lentivirus expressing scrambled (Scr) or SIRT1 (T1) small hairpin RNA (shRNA) (n = 8).

(F) Number of migrated HAECs (n = 8).

Data are expressed as mean \pm SEM. *p < 0.05, **p < 0.005, ***p < 0.0005, δ p < 0.00005 by Student's t test (C), one-way (D–F), or two-way (A and B) ANOVA with Bonferroni's corrections.

See also Figure S3.

process, we first subjected 10-month-old inducible SIRT1 knockout mice (SIRT1-iKO) (Figure S2N) (Price et al., 2012) to a 4-week treadmill training paradigm. Immediately after SIRT1 deletion, there was no difference in capillary number or density. After 4 weeks of exercise training, however, the number of capillaries and capillary density in the quadriceps muscle of SIRT1-iKO mice was only 1.4-fold higher compared to 2-fold in WT mice (Figure 2G), indicating that SIRT1 is required for exercise-induced muscle neovascularization.

PGC-1 α increases mitochondrial function and induces the secretion of VEGF to promote neovascularization (Arany et al., 2008). Indeed, mice lacking PGC-1 α have limited angiogenesis after exercise (Chinsomboon et al., 2009) whereas mice overexpressing PGC-1 α in muscle have increased mitochondria and capillary density (Lin et al., 2002). We deleted SIRT1 either in ECs or myocytes of the muscle-specific PGC-1 α overexpressing mouse (MCK-PGC-1 α). Despite there being no effect on mitochondrial protein levels (Figures

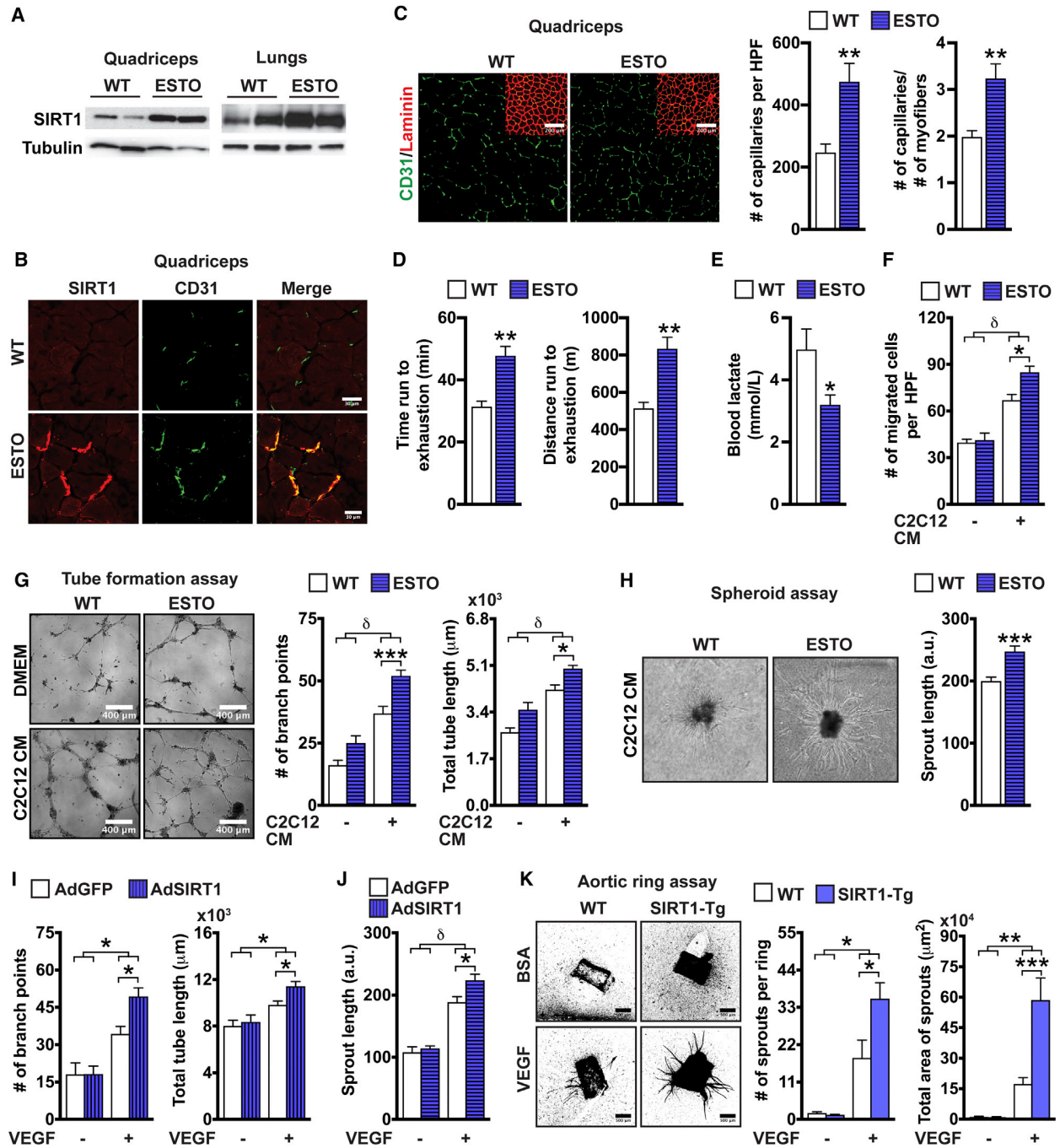


Figure 4. Endothelial SIRT1 Increases Capillary Density and Exercise Capacity

(A) SIRT1 protein abundance in quadriceps and lungs. Tubulin serves as a loading control.
 (B) Quadriceps sections (60×) showing SIRT1 and CD31 expression.
 (C) Quadriceps sections (20×) showing CD31 and laminin staining. Number of capillaries and capillary/fiber ratio (6-month-old, n = 8).
 (D) Duration and distance run until exhaustion in a high intensity treadmill test (6-month-old, n = 8).
 (E) Post-exercise blood lactate levels (n = 5).
 (F) Number of migrated MLECs (n = 10).
 (G) Images, number of branch points, and length of tube networks formed by MLECs (n = 8).
 (H) Images and sprout length of MLEC spheroids (n = 8-9).
 (I) Images, number of branch points, and length of tube networks formed by HUVECs infected with adenovirus expressing GFP or SIRT1 (n = 8-9).

(legend continued on next page)

S2O and S2P), *MCK-PGC-1 α ;ESKO* mice had significantly reduced capillary density compared to *MCK-PGC-1 α ;WT* mice (Figure 2H). As shown in Figure 2I, the presence or absence of SIRT1 in myocytes made no difference in the number of capillaries induced by PGC-1 α . Together, these data indicate that SIRT1 in ECs, but not myocytes, is a critical downstream mediator of PGC-1 α -induced signals originating from myofibers. In treadmill tests, *MCK-PGC-1 α ;ESKO* mice had greatly reduced endurance compared to *MCK-PGC-1 α* mice (Figure 2J) but not in the *MCK-PGC-1 α ;MSKO* mice (Figure 2K). Thus, SIRT1 in ECs is required for PGC-1 α to improve exercise tolerance, even if mitochondrial function is already higher, underscoring the critical role of the vasculature SIRT1 in endurance.

SIRT1 Is Required for Pro-angiogenic Growth Factor Signaling from Myocytes to ECs

To investigate the specific signals that EC SIRT1 responds to, we performed *in vitro* transwell migration and spheroid assays using MLECs derived from WT and ESKO mice. MLECs without SIRT1 had a blunted chemotactic response (Figures 3A and S3A), reduced tube formation (Figure 3B), and shorter EC spheroid sprout length (Figure 3C). Stimulation of EC replication and migration after exercise involves several pro-angiogenic factors including VEGF and basic fibroblast growth factor (FGF) (Arany et al., 2008). To determine if growth factors require SIRT1 activity, we examined aortic rings from WT and SIRT1-iKO mice that were exposed to either VEGF or FGF (Figures 3D and S3B). Stimulation of sprouting was reduced in the aortic rings lacking SIRT1 (Figures 3D and S3C). SIRT1-deficient human aortic ECs (HAECs) (Figure S3D) also had a reduced response to growth factors (Figures 3E and 3F). SIRT1 had no effect on VEGF mRNA or VEGF protein in serum (Figures S3E and S3F).

Increasing Endothelial SIRT1 Activity Increases Muscle Capillary Density and Exercise Capacity

Having found that endothelial SIRT1 is necessary for vascular remodeling, we tested if increasing its abundance or activity was sufficient. To test this, an EC-specific SIRT1 overexpressing mouse strain (ESTO (Figures 4A, 4B, S4A, and S4B) was generated. There were no apparent physical abnormalities (Figures S4C–S4E) or differences in mitochondria (Figures S4D–S4H) but interestingly, blood glucose levels were reduced related to WT (Figure S4I), indicating that endothelial SIRT1 may promote glucose uptake or suppress gluconeogenesis.

Compared to littermate controls, the density and number of capillaries in the quadriceps of ESTO mice was 1.5-fold and 2-fold greater, respectively (Figure 4C), with similar increases in gastrocnemius (Figure S4J). Relative to WT, 6-month-old

ESTO mice ran 1.8 times longer and covered 1.9 times the distance before exhaustion (Figure 4D; Movie S2), and even had lower post-exercise serum lactate (Figure 4E). Thus, increasing the expression of SIRT1 in ECs is sufficient to increase the capillary density of skeletal muscle and enhance exercise performance.

If endothelial SIRT1 is a downstream mediator of angiogenic signals from myocytes (see Figures 2 and 3), increasing endothelial SIRT1 should augment these signals. Overexpression of SIRT1 in MLECs increased cell motility (Figure 4F), tube formation, and sprout length of EC spheroids (Figures 4G and 4H). Overexpression of SIRT1 in human umbilical vein ECs (HUVECs) increased the number of branching points by 33% and the total tubule length by 15% compared to the control cells (Figures 4I, S4K, and S4L). In a spheroid assay, adeno-SIRT1 infected ECs had 19% longer sprout lengths compared to the control cells upon VEGF stimulation (Figures 4J and S4M). Aortic rings from whole body SIRT1 overexpressing mice (SIRT1-Tg) (Figure S4N) had double the sprout number and triple the total sprout area (Figure 4K). ESTO mice had higher VEGF serum protein levels (Figure S4O), indicating SIRT1 is part of a positive feedback pathway sensitizing myocytes to VEGF and is both necessary and sufficient for skeletal muscle capillary formation.

The NAD⁺ Precursor, NMN, Promotes Angiogenesis by Inhibiting SIRT1-Mediated Notch Signaling

The loss of exercise responsiveness in older mice might have been due to a decline in SIRT1 or the levels of its co-substrate NAD⁺ (Gomes et al., 2013). NAD⁺ precursors are an effective way to raise intracellular NAD⁺ levels and stimulate SIRT1 activity (Bogan and Brenner, 2008; Gomes et al., 2013; Yoshino et al., 2011). In cell migration, sprouting and tube formation assays (Figures 5A–5D and S5A–S5D) NMN increased angiogenesis in a SIRT1-dependent manner, significantly improving tubule structure while preventing tube disintegration (Movies S3 and S4). NMN also doubled the number of outgrowths or sprouts from aortic rings taken from 18-month-old WT mice but not old SIRT1-iKOs (Figures 5E and S5E). SIRT3 and SIRT6 also increase the angiogenic potential of ECs in culture (Cardus et al., 2013; Wei et al., 2017). Knockdown of SIRT3 and SIRT6 in HAECs decreased tube formation and spheroid sprouting that was partially rescued by NMN (Figures S5F–S5H), indicating that its angiogenic effects are primarily mediated by SIRT1.

In vertebrates, the Notch signaling pathway is indispensable for blood vessel formation (Blanco and Gerhardt, 2013). Notch signaling in ECs is controlled by the Notch1 intracellular domain (NICD) protein, which in turn is negatively regulated by SIRT1 (Guarani et al., 2011). After stimulation with VEGF or Notch ligand Dll4 (Figures 5F and S5I), NMN treatment decreased

(J) Sprout length of HUVEC spheroids (n = 8).

(K) Images, number, and total area of microvessel sprouts in aortic rings (n = 9).

Data expressed as mean \pm SEM. *p < 0.05, **p < 0.005, ***p < 0.0005, [§]p < 0.00005 by Student's t test (C–E and H) or two-way ANOVA with Bonferroni's corrections (F, G, and I–K).

See also Figure S4 and Movie S2.

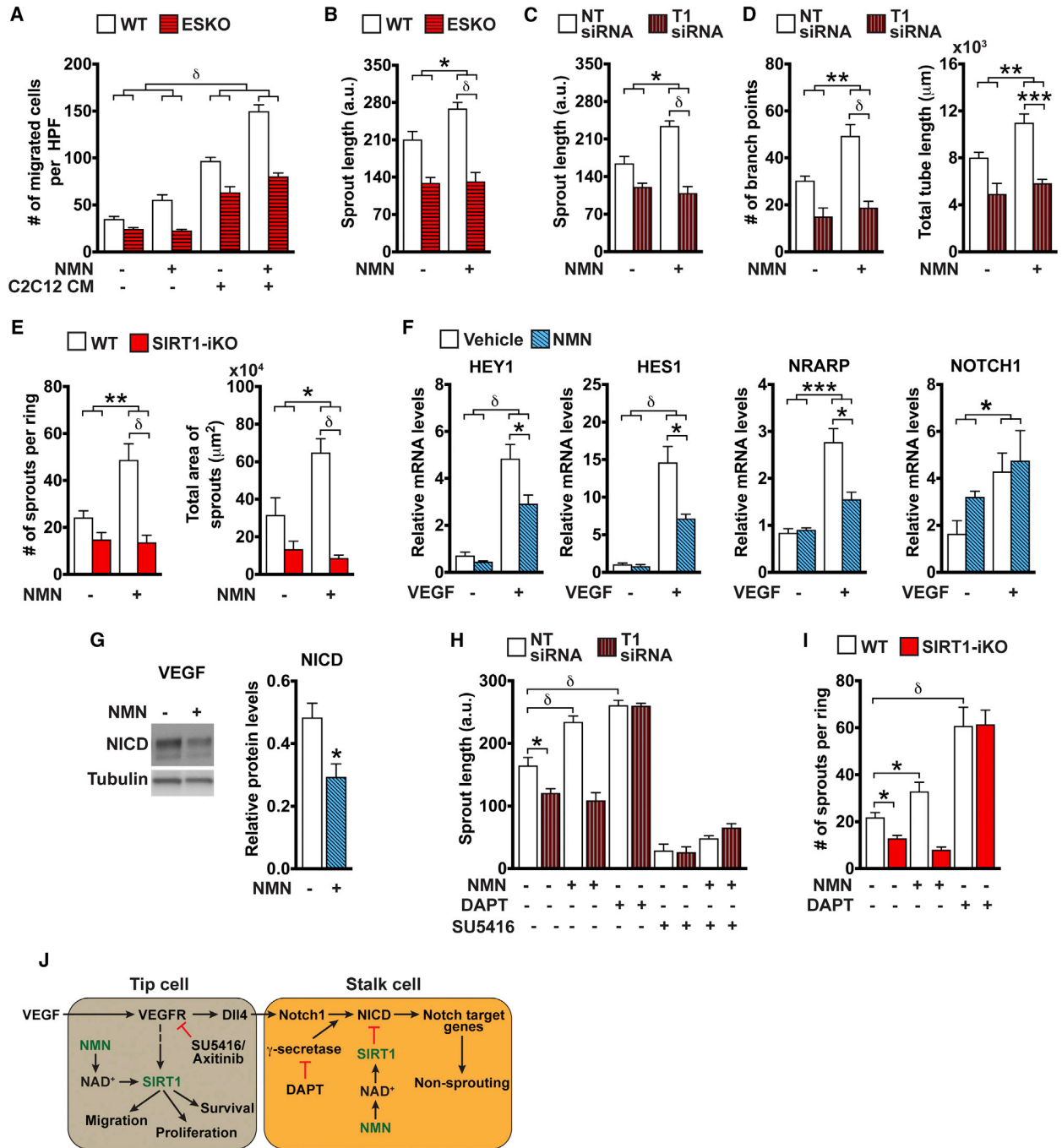


Figure 5. Endothelial NAD⁺ Sensitizes ECs to VEGF by Suppressing Notch

- (A) Number of migrated MLECs (n = 12).
 (B) Sprout length of MLEC spheroids (n = 8).
 (C) Sprout length of HAEC spheroids transfected with non-targeting (NT) or SIRT1 (T1) small interfering RNAs (siRNAs) (n = 8).
 (D) Number of branch points and length of HAEC tube networks (n = 13).
 (E) Number and total area of sprouts originating from aortic rings (18-month-old, n = 8).
 (F) Relative mRNA levels of Notch target genes (HEY1, HES1, and NRARP) and NOTCH1 in HAECs stimulated with VEGF for 1 hr (n = 4).
 (G) Notch Intracellular Domain (NICD) protein and relative abundance in HAECs stimulated with VEGF for 5 hr (n = 3).
 (H) Sprout length of VEGF-stimulated HAEC spheroids transduced with NT or T1 siRNAs (n = 8).
 (I) Number of sprouts in VEGF-stimulated aortic rings (18-month-old, n = 8).

(legend continued on next page)

Notch target gene expression and NICD protein levels (Figures 5G and S5J). Blocking NICD release with the γ -secretase inhibitor DAPT increased sprout length irrespective of SIRT1 levels (Figures 5H, 5I, and S5K) while treatment with the VEGF receptor inhibitor SU5416 completely blocked sprouting and this was not rescued by NMN treatment (Figure 5H). NMN treatment induced proliferation (Figure S5L) and reduced apoptosis in ECs in a SIRT1-dependent manner, consistent with an inhibition of Notch (Noseda et al., 2004) (Figure S5M). Thus, Notch signaling in ECs depends on NAD⁺ levels and the concomitant activity of SIRT1 (Figure 5J).

NAD⁺ Reverses Loss of the Microvasculature and Exercise Capacity in Old Mice via SIRT1

During aging, the level of NAD⁺ declines in many tissues, in part, due to increased activity of the NAD-consuming enzymes CD38 and PARP1 (Bai et al., 2011b; Camacho-Pereira et al., 2016; Li et al., 2017; Mouchiroud et al., 2013). We hypothesized that decreasing NAD⁺ levels in ECs might explain why older individuals have fewer capillaries and decreased blood flow. Gastrocnemius muscle and ECs isolated from 20-month-old mice had lower NAD⁺ levels compared to those from 6-month-olds (Figure 6A). We reasoned, therefore, that restoring NAD⁺ levels in ECs of old mice to youthful levels might also restore capillary density, blood flow, and endurance. To restore NAD⁺ levels, we administered NMN to 18-month-old mice via drinking water for 2 months at 400 mg/kg/day (Figures S6A–S6C).

NMN restored the number of capillaries and capillary density of the old mice to those typically seen in young mice (Figures 6B and S6D). Resting muscle perfusion (Figures 6C and S6E) and soluble oxygen (sO₂) levels were significantly higher in NMN-treated mice compared to controls (Figure 6D). Mitochondrial protein and activity levels and other muscle properties remained unaltered (Figures S6F–S6L). NMN supplementation dramatically increased home-cage oxygen consumption (Figure S6M), but the most striking effect was a 56%–80% improvement in endurance, with lower post-exercise blood lactate (Figures 6E and 6F; Movie S5).

To test if SIRT1 is necessary for neovascularization *in vivo*, 20-month-old tamoxifen-treated WT and SIRT1-iKO mice were treated with NMN for 2 months. NMN increased gastrocnemius capillarity in WT but not in the SIRT1-iKO mice (Figure 6G). Angiogenesis is also important for tissues to recover from ischemia. NMN restored blood volume and capillary density in a SIRT1-dependent manner in mice subjected to femoral artery ligation (Figures 6H and S6N).

NMN did not alter the capillarity or exercise capacity of sedentary animals younger than 12 months (not shown), consistent

with overexpression of Nampt, an NAD biosynthetic gene (Fredrick et al., 2015). There was a strong effect, however, in young mice on NMN after endurance training for 1 month, resulting in 70% more capillaries than untreated sedentary mice, more than twice the effect of NMN alone (Figure 6I). To test if NMN works by sensitizing ECs to VEGF, we treated mice with axitinib, an inhibitor of VEGF signaling (Figure S6O) and saw no effect of NMN on capillary density and exercise capacity (Figures 6J and S6P).

Exogenous Hydrogen Sulfide Activates SIRT1 and Augments the Effects of NMN

As a signaling molecule, H₂S shares many similarities with NAD⁺. It increases SIRT1 activity, protects against oxidative stress, and can promote angiogenesis (Longchamp et al., 2018). Treatment of HUVECs with NaHS or NMN alone increased SIRT1 protein levels but the combination was even more potent (Figure 7A). NaHS increased intracellular NAD⁺ levels, MLECs motility (Figures 7B and 7C) and spheroid sprouting (Figures 7D and S7A), an effect that was SIRT1-dependent (Figure 7C). Consistent with Longchamp et al. (2018), H₂S increased cell migration independently of VEGF but dependent on SIRT1 (Figure S7B), while lowering basal OCR while NMN did not (Figure S7C). These findings indicate that NAD⁺ and H₂S have overlapping and distinct functions in ECs.

To test the effects of the NMN-NaHS combination, we co-treated 32-month-old mice with NMN and NaHS for 4 weeks (Figure S7D). The combination of NaHS and NMN dramatically increased capillary density compared to other treatment groups (Figure 7E). Neovascularization declines during aging, in part, because of an increase in oxidative stress and EC apoptosis (Dimmeler and Zeiher, 2000; Pearson et al., 2008). In response to H₂O₂ treatment, NMN reduced the number of apoptotic ECs from 42% to 17% and, in combination with NaHS, reduced it to 11% (Figures 7F and S7E). NMN also reduced apoptosis in HUVECs by 13% and the combination reduced it by 36% (Figures 7G and S7F). Mice treated with NMN had 1.6-fold increase in time and distance run compared to untreated mice (Figure 7H), while the combination of NMN with NaHS treatment doubled their endurance.

The reduced baseline capillary density of ESKO mice confounded the interpretation of the effects of NMN and NaHS. To circumvent this, we knocked down SIRT1 in old mice using a lentivirus expressing SIRT1 miRNA downstream of the vascular endothelium cadherin (VE-cad) promoter (Figure S7G; Table S1) (Zhang et al., 2013). The most efficient miRNA virus was #5, which knocked down SIRT1 80% and raised NICD (Figures 7I and S7H). SIRT1 was knocked down in 20-month-old mice (Figures 7J and S7I) that were then

(J) VEGF stimulation during sprouting angiogenesis upregulates expression of Dll4 ligand in the tip cells, activating Notch in the stalk cells, which triggers proteolytic cleavage of Notch receptor by γ -secretase complex to release NICD from the cell membrane so it translocates to the nucleus and induces transcription of target genes. Activation of SIRT1 by the NAD booster NMN promotes migration, proliferation, and survival in VEGF-stimulated ECs. In stalk cells, NMN suppresses NICD during VEGF/Dll4 stimulation and Notch target gene activation, thereby promoting sprouting. VEGF receptor inhibitors SU5416 or axitinib block the effects of NMN on angiogenesis.

Data expressed as mean \pm SEM. *p < 0.05, **p < 0.005, ***p < 0.0005, [§]p < 0.00005 by Student's t test (G), one-way (H and I), or two-way (A–F) ANOVA with Bonferroni's corrections.

See also Figure S5 and Movies S3 and S4.

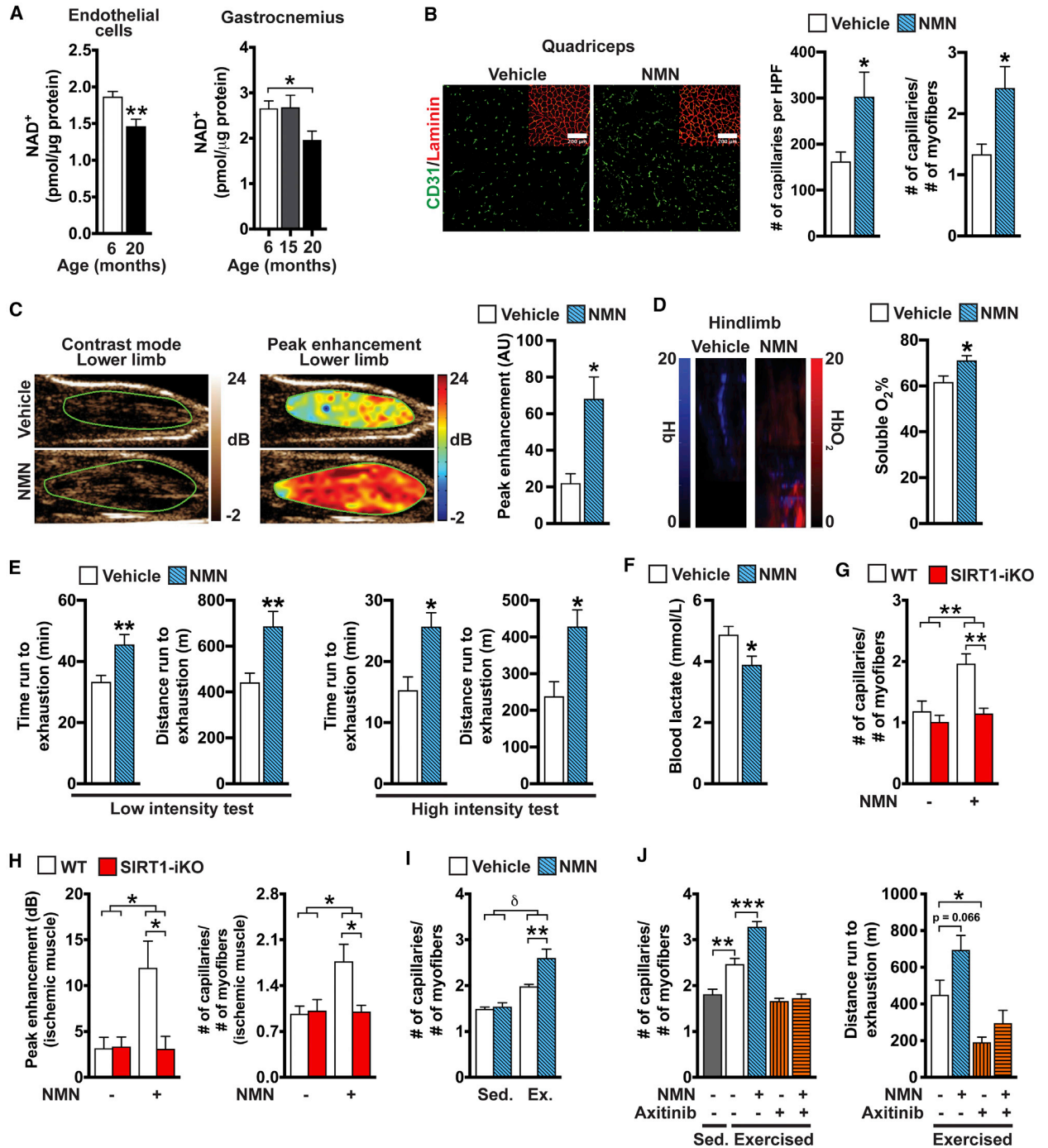


Figure 6. NAD Repletion Restores the Microvasculature and Exercise Capacity of Old Mice

(A) NAD⁺ levels in MLECs (n = 6) and gastrocnemius muscles (n = 10) isolated from 6- and 20-month-old mice.
 (B) Quadriceps sections (20×) from 20-month-old vehicle or NMN-treated mice showing CD31 and laminin staining. Number of capillaries and capillary/myofiber ratio (n = 8).
 (C) Contrast-mode and peak enhancement-mode contrast-enhanced ultrasound images of mouse hindlimb. Quantification of peak enhancement (20-month-old, n = 5).
 (D) Total hemoglobin (Hb) and oxygenated Hb (HbO₂) mean intensity in the hindlimbs of mice measured using photoacoustics tomography. Percent soluble O₂ levels (n = 13).
 (E) Duration and distance run until exhaustion (20-month-old, n = 13).

(legend continued on next page)

treated for 4 weeks with NMN and/or H₂S precursors (NaHS and GYY4137). The ability of NMN alone or in combination with H₂S precursors to increase vascularization was blocked in the SIRT1 knockdown mice (Figure 7K). Although the system may result in off-target effects and produce short-term effects making it difficult to directly compare them to knockout mice, they are consistent with our previous conclusions that raising NAD⁺ levels and stimulating SIRT1 activity in ECs is an effective way to increase angiogenesis and blood flow to improve exercise endurance, a pathway that is further enhanced by co-treatment with H₂S (Figure S7L).

DISCUSSION

From the age of 40 onward, the tissue perfusion declines steadily and seemingly inexorably, leading to organ dysfunction and increasing frailty in the last decades of life (Degens, 1998; Le Couteur and Lakatta, 2010). Although exercise is recommended, it only delays a cycle of decline, both physically and physiologically (Denis et al., 1986). In this study, we show that a decrease in endothelial NAD⁺ is a primary reason why our ability to exercise and receive its benefits diminish as we age. Specifically, endothelial NAD⁺ and SIRT1 are critical regulators of vascular remodeling in response to VEGF-stimulated angiogenesis. NMN restores angiogenesis in old mice ostensibly via a SIRT1-regulated Notch signaling pathway, underscoring the importance of Notch signaling in aging. At 32 months of age, the effects of aging on the mouse microvasculature were surprisingly easy to reverse. As far as we are aware, this is the first time a small molecule has induced neovascularization at an advanced age.

Interestingly, NMN supplementation had no effect on the capillary density of sedentary young to middle-aged mice. Only when coupled with exercise training or after ischemia did NMN improve these parameters. This result, and the fact that NMN restores the capillary density of elderly mice to youthful levels but not further, indicates that there may be a signal within EC that caps the number of capillaries in muscle that EC NAD⁺ can induce, a limit that is overcome by exercise. If this putative factor is found, it could have significant implications for human health. A potential candidate is CBP/p300-interacting transactivator with ED-rich tail 2 (CITED2), an inhibitor of hypoxia-inducible factor 1 (HIF-1 α) signaling that is implicated in type 2 diabetes (Wang et al., 2016). It would be interesting to test whether exercise inhibits expression of CITED2 and if NMN requires CITED2 to increase angiogenesis.

Increasing SIRT1 activity has been thought to improve endurance capacity by increasing mitochondrial function (Bai et al., 2011a, 2011b; Baur et al., 2006; Cantó et al., 2009; Lagouge

et al., 2006; Pearson et al., 2008). Challenging this assumption, there were no changes in the muscle oxidative capacity in ESTO or NMN-treated mice, despite a dramatic increase in endurance. Conversely, increasing muscle oxidative capacity was insufficient to improve endurance in the absence of increased capillarity, indicating the modes by which SIRT1 activators or NAD boosters increase exercise endurance should be reexamined. Although we saw no change in cardiac function or capillary density, we cannot rule out the possibility of cardiac changes.

The ability of NMN to promote angiogenesis raises the question of whether it might stimulate tumor growth. Mice treated with NMN or NR for extended periods show no evidence of increased tumor burden (Mills et al., 2016; Zhang et al., 2016). Indeed, during the course of our studies, no increase in tumor burden was seen with NMN-treatment or in a DEN-induced model of hepatocarcinoma (Figures S7J and S7K), although more study is warranted.

A major cause of age-associated endothelial dysfunction is an increase in oxidative stress and apoptosis (Harman, 1956). SIRT1 and H₂S protect against oxidative stress-mediated apoptosis and senescence (Miller and Roth, 2007; Salminen et al., 2013; Suo et al., 2013; Wu et al., 2015). We suggest that in response to exercise, a SIRT1-H₂S pathway within ECs prevents apoptosis after oxidative stress and sensitizes the cells to PGC-1 α -mediated VEGF secretion (Figure S7L). During aging, however, NAD⁺ levels decline in ECs, leading to a reduction in SIRT1 activity and the ability of ECs to survive oxidative stress and respond to growth factor signaling. The age-associated increase in oxidative stress further reduces SIRT1 expression, exacerbating the decline.

Skeletal muscle is not the only tissue that requires adequate blood flow to maintain function. Heart, liver, bone, and the brain, for example, are critically dependent on blood flow. It will be interesting to test whether upregulation of the endothelial NAD⁺-H₂S pathway improves the vasculature and blood flow into those tissues as well. If so, precursors to NAD⁺ and H₂S may not only be effective agents for increasing the recovery from vessel blockages and enhancing the effects of exercise, but also for treating the most common of age-related diseases, if not aging itself.

STAR★METHODS

Detailed methods are provided in the online version of this paper and include the following:

- KEY RESOURCES TABLE
- CONTACT FOR REAGENT AND RESOURCES SHARING

(F) Post-exercise blood lactate levels (20-month-old, n = 13).

(G) Capillary/myofiber ratio in gastrocnemius sections (20-month-old, n = 5).

(H) Peak enhancement and capillary/myofiber ratio for ischemic hindlimbs (8-month-old, n = 5).

(I) Capillary/myofiber ratio in quadriceps of sedentary or exercised mice (10-month-old, n = 5).

(J) Capillary/myofiber ratio in quadriceps (5-month-old, n = 5). Distance run until exhaustion at the end of the exercise paradigm (n = 5).

Data are expressed as mean \pm SEM. *p < 0.05, **p < 0.005, ***p < 0.0005, [§]p < 0.00005 by Student's t test (A–F), one-way (J), or two-way (G–I) ANOVA with Bonferroni's corrections.

See also Figure S6 and Movie S5.

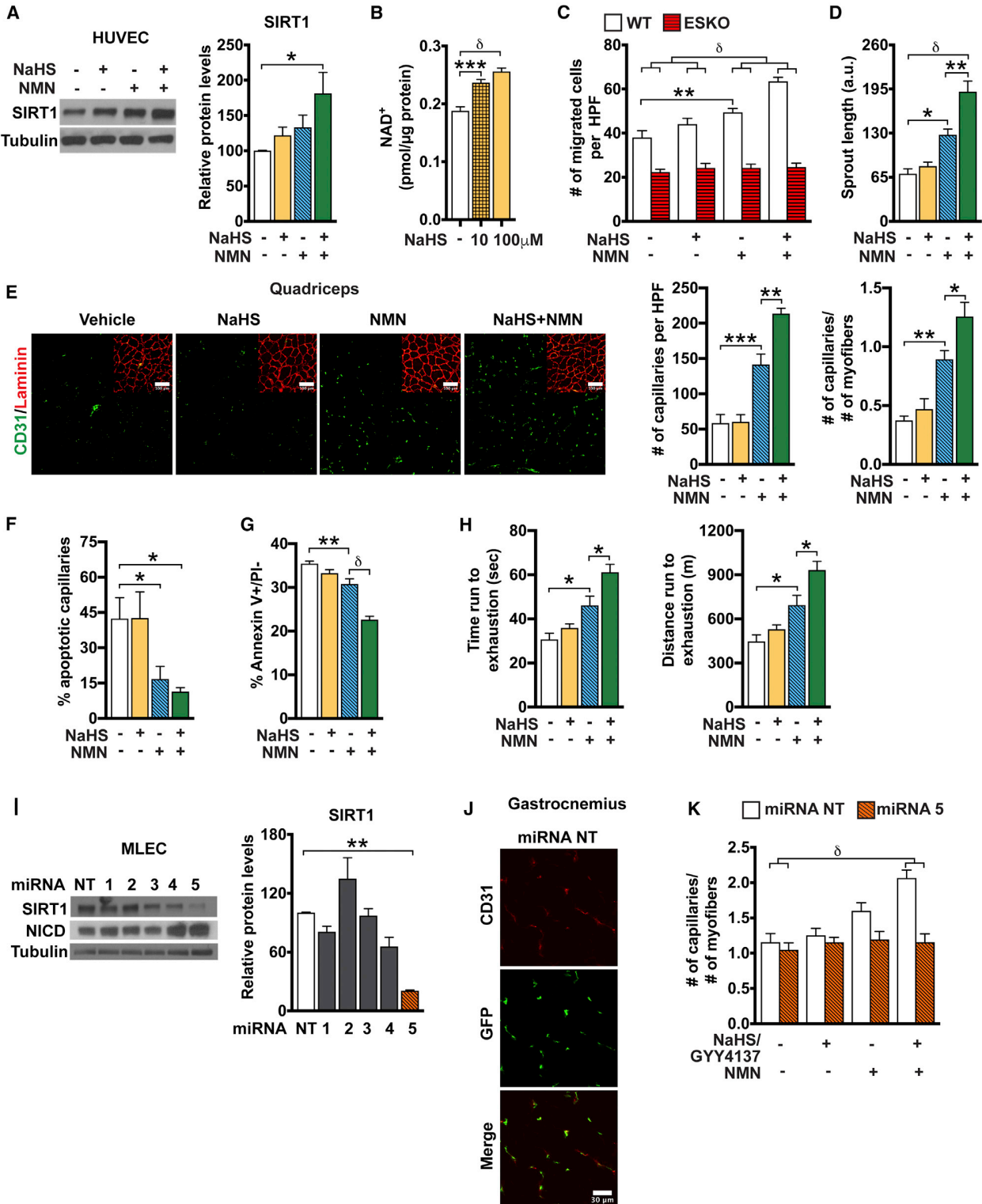


Figure 7. Exogenous Hydrogen Sulfide Activates SIRT1 and Augments the Effects of NMN

(A) SIRT1 protein and relative abundance in HUVECs treated for 24 hr (n = 4).

(B) NAD⁺ levels in HUVECs treated for 24 hr (n = 6).

(legend continued on next page)

● EXPERIMENTAL MODEL AND SUBJECT DETAILS

- Animals
- Cells

● METHOD DETAILS

- Endurance testing of mice
- Exercise training of mice
- Blood glucose, lactate and VEGF
- Urine creatinine
- Rotarod test
- Hindlimb ischemia
- Contrast-enhanced ultrasound (CEU)
- Cardiac ultrasound
- Photoacoustic imaging
- Metabolic measurements and body composition
- Permeabilized fiber respiration
- Enzyme activity assays
- NAD⁺ measurements
- Genotyping PCR analysis
- Primary mouse EC (MLEC) isolation
- Measurement of percent skeletal muscle ECs
- RNA interference and viral infection
- Dll4 and VEGF stimulation of ECs
- Construction of miRNA vectors and lentivirus production
- C2C12 Conditioned Media (CM)
- Transwell migration assay

● TUBE FORMATION ASSAY

- Spheroid assay
- Aortic ring assay
- Wound scratch assay
- Proliferation assay
- Apoptosis assay
- Seahorse analysis
- Immunofluorescence
- Hematoxylin and eosin (H&E) staining
- RNA analysis
- Western

● QUANTIFICATION AND STATISTICAL ANALYSIS

SUPPLEMENTAL INFORMATION

Supplemental Information includes seven figures, two tables, and five movies and can be found with this article online at <https://doi.org/10.1016/j.cell.2018.02.008>.

(C) Number of migrated MLECs stimulated with C2C12 CM for 12 hr (n = 15).

(D) Sprout length of VEGF-stimulated HUVEC spheroids (n = 7).

(E) Quadriceps sections (20×) showing CD31 and laminin staining. Capillary number and capillary/myofiber ratio (32-month-old, n = 7).

(F) Percent TUNEL⁺ capillaries in quadriceps sections (32-month-old, n = 5).

(G) Number of apoptotic HUVECs (Annexin V⁺/PI⁻) following exposure to H₂O₂ (n = 12).

(H) Duration and distance run until exhaustion in a low intensity treadmill test (32-month-old, n = 7).

(I) SIRT1 and NICD proteins in MLECs transduced with lentiviruses expressing NT or SIRT1 miRNAs (miRNA #1–5). Relative SIRT1 protein abundance (n = 3).

(J) Images of gastrocnemius sections (40×) immunostained with EGFP and CD31 from WT mice injected with lentiviral particles that transduced EGFP and NT miRNA.

(K) Capillary/myofiber ratio in the gastrocnemii of mice infected with lentiviral particles transducing NT or SIRT1 #5 miRNA (n = 6).

Data are expressed as mean ± SEM. *p < 0.05, **p < 0.005, ***p < 0.0005, ^δp < 0.00005 by Student's t test (I), one-way (A, B, and D–H), or two-way (C and K) ANOVA with Bonferroni's corrections.

See also [Figure S7](#) and [Table S1](#).

ACKNOWLEDGMENTS

We thank Margaret Morris, Edna Hardeman, Doyle Lokitayakul, Patty Lee, Yi Zhang, Kyle Hoehn, Anthony Kee, Neil Youngson, Golam Mezbah Uddin, Corrine Fiveash, Ellen Olzomer, Menghan Liu, Nicholas Bentley, NIF-BMIF-BRIL-BRC (UNSW), and Paul Glenn for support. This work was supported by the Glenn Foundation for Medical Research (RO1 AG028730 and RO1 DK100263), the Sinclair Gift Fund, a gift from Edward Schulak to D.A.S., NIH/NIA (RO1 AG015339) to L.G., and NIH/NHLBI (RO1 HL094499) to Z.A. **Q1** This study is dedicated to Vera Ryan, grandmother to D.A.S., who believed the measure of a person is not their status or wealth but their impact.

AUTHOR CONTRIBUTIONS

Management, A.D., L.G., L.E.W., Z.A., and D.A.S.; Experimental Design, A.D., G.X.H., Z.A., J.R.M., A.L., and D.A.S.; ESKO, ESTO, and Pharmacology, A.D., M.S.B., M.B.S., L.-J.K., C.L., B.O., S.J., J.H.T.-V., Y.L., M.-J.K., and N.T.; PGC-1 α , G.X.H. and Z.A.; Imaging, A.D., T.H., and B.L.; Resources, A.L., E.O.W., M.I., J.R.M., L.E.W., L.G., Z.A., and D.A.S.; Manuscript, Rebuttal, Revisions, A.D. and D.A.S.; Funding, L.G., Z.A., L.E.W., and D.A.S.

DECLARATION OF INTERESTS

D.A.S. and L.E.W. are both consultants/inventors on patents licensed to Metro International Biotech, Jumpstart Fertility, Life Biosciences, and Liberty Biosecurity and D.A.S. is to EdenRoc Sciences, ArcBio, Segterra, Animal Biosciences, Senolytic Therapeutics, Spotlight Biosciences, and Continuum Biosciences. L.E.W. is a consultant to Intravital and Jumpstart Fertility. M.S.B. is a consultant to Metro International Biotech. L.G. is an advisor to Segterra, Sebelius, and Elysium Health. A provisional patent application has been submitted with A.D., L.E.W. and D.A.S. as inventors. The other authors declare no competing interests.

Received: October 9, 2017

Revised: December 25, 2017

Accepted: January 31, 2018

Published: March 22, 2018

REFERENCES

Arany, Z., Foo, S.Y., Ma, Y., Ruas, J.L., Bommi-Reddy, A., Girmun, G., Cooper, M., Laznik, D., Chinsomboon, J., Rangwala, S.M., et al. (2008). HIF-independent regulation of VEGF and angiogenesis by the transcriptional coactivator PGC-1 α . *Nature* *451*, 1008–1012.

Bai, P., Canto, C., Brunyánszki, A., Huber, A., Szántó, M., Cen, Y., Yamamoto, H., Houten, S.M., Kiss, B., Oudart, H., et al. (2011a). PPAR-2 regulates SIRT1 expression and whole-body energy expenditure. *Cell Metab.* *13*, 450–460.

Bai, P., Cantó, C., Oudart, H., Brunyánszki, A., Cen, Y., Thomas, C., Yamamoto, H., Huber, A., Kiss, B., Houtkooper, R.H., et al. (2011b). PPAR-1 inhibition increases mitochondrial metabolism through SIRT1 activation. *Cell Metab.* *13*, 461–468.

- Baker, M., Robinson, S.D., Lechertier, T., Barber, P.R., Tavora, B., D'Amico, G., Jones, D.T., Vojnovic, B., and Hodivala-Dilke, K. (2011). Use of the mouse aortic ring assay to study angiogenesis. *Nat. Protoc.* 7, 89–104.
- Baltgalvis, K.A., White, K., Li, W., Claypool, M.D., Lang, W., Alcántara, R., Singh, B.K., Frier, A.M., McLaughlin, J., Hansen, D., et al. (2014). Exercise performance and peripheral vascular insufficiency improve with AMPK activation in high-fat diet-fed mice. *Am. J. Physiol. Heart Circ. Physiol.* 306, H1128–H1145.
- Bassel-Duby, R., and Olson, E.N. (2006). Signaling pathways in skeletal muscle remodeling. *Annu. Rev. Biochem.* 75, 19–37.
- Baur, J.A., Pearson, K.J., Price, N.L., Jamieson, H.A., Lerin, C., Kalra, A., Prabhu, V.V., Allard, J.S., Lopez-Lluch, G., Lewis, K., et al. (2006). Resveratrol improves health and survival of mice on a high-calorie diet. *Nature* 444, 337–342.
- Blanco, R., and Gerhardt, H. (2013). VEGF and Notch in tip and stalk cell selection. *Cold Spring Harb. Perspect. Med.* 3, a006569.
- Bogan, K.L., and Brenner, C. (2008). Nicotinic acid, nicotinamide, and nicotinamide riboside: a molecular evaluation of NAD⁺ precursor vitamins in human nutrition. *Annu. Rev. Nutr.* 28, 115–130.
- Booth, F.W., and Thomason, D.B. (1991). Molecular and cellular adaptation of muscle in response to exercise: perspectives of various models. *Physiol. Rev.* 71, 541–585.
- Borradaile, N.M., and Pickering, J.G. (2009). Nicotinamide phosphoribosyltransferase imparts human endothelial cells with extended replicative lifespan and enhanced angiogenic capacity in a high glucose environment. *Aging Cell* 8, 100–112.
- Camacho-Pereira, J., Tarragó, M.G., Chini, C.C.S., Nin, V., Escande, C., Warner, G.M., Puranik, A.S., Schoon, R.A., Reid, J.M., Galina, A., and Chini, E.N. (2016). CD38 dictates age-related NAD decline and mitochondrial dysfunction through an SIRT3-dependent mechanism. *Cell Metab.* 23, 1127–1139.
- Cantó, C., Gerhart-Hines, Z., Feige, J.N., Lagouge, M., Noriega, L., Milne, J.C., Elliott, P.J., Puigserver, P., and Auwerx, J. (2009). AMPK regulates energy expenditure by modulating NAD⁺ metabolism and SIRT1 activity. *Nature* 458, 1056–1060.
- Cantó, C., Houtkooper, R.H., Pirinen, E., Youn, D.Y., Oosterveer, M.H., Cen, Y., Fernandez-Marcos, P.J., Yamamoto, H., Andreux, P.A., Cettour-Rose, P., et al. (2012). The NAD⁺ precursor nicotinamide riboside enhances oxidative metabolism and protects against high-fat diet-induced obesity. *Cell Metab.* 15, 838–847.
- Cantó, C., Menzies, K.J., and Auwerx, J. (2015). NAD⁺ metabolism and the control of energy homeostasis: a balancing act between mitochondria and the nucleus. *Cell Metab.* 22, 31–53.
- Cardus, A., Uryga, A.K., Walters, G., and Erusalimsky, J.D. (2013). SIRT6 protects human endothelial cells from DNA damage, telomere dysfunction, and senescence. *Cardiovasc. Res.* 97, 571–579.
- Cheng, H.L., Mostoslavsky, R., Saito, S., Manis, J.P., Gu, Y., Patel, P., Bronson, R., Appella, E., Alt, F.W., and Chua, K.F. (2003). Developmental defects and p53 hyperacetylation in Sir2 homolog (SIRT1)-deficient mice. *Proc. Natl. Acad. Sci. USA* 100, 10794–10799.
- Chinsomboon, J., Ruas, J., Gupta, R.K., Thom, R., Shoag, J., Rowe, G.C., Sawada, N., Raghuram, S., and Arany, Z. (2009). The transcriptional coactivator PGC-1 α mediates exercise-induced angiogenesis in skeletal muscle. *Proc. Natl. Acad. Sci. USA* 106, 21401–21406.
- de Picciotto, N.E., Gano, L.B., Johnson, L.C., Martens, C.R., Sindler, A.L., Mills, K.F., Imai, S., and Seals, D.R. (2016). Nicotinamide mononucleotide supplementation reverses vascular dysfunction and oxidative stress with aging in mice. *Aging Cell* 15, 522–530.
- Degens, H. (1998). Age-related changes in the microcirculation of skeletal muscle. *Adv. Exp. Med. Biol.* 454, 343–348.
- Denis, C., Chatard, J.C., Dormois, D., Linossier, M.T., Geyssant, A., and Lacour, J.R. (1986). Effects of endurance training on capillary supply of human skeletal muscle on two age groups (20 and 60 years). *J. Physiol. (Paris)* 87, 379–383.
- Dimmeler, S., and Zeiher, A.M. (2000). Endothelial cell apoptosis in angiogenesis and vessel regression. *Circ. Res.* 87, 434–439.
- Escudier, B., and Gore, M. (2011). Axitinib for the management of metastatic renal cell carcinoma. *Drugs R D* 11, 113–126.
- Firestein, R., Blander, G., Michan, S., Oberdoerffer, P., Ogino, S., Campbell, J., Bhimavarapu, A., Luikenuis, S., de Cabo, R., Fuchs, C., et al. (2008). The SIRT1 deacetylase suppresses intestinal tumorigenesis and colon cancer growth. *PLoS ONE* 3, e2020.
- Frederick, D.W., Davis, J.G., Dávila, A., Jr., Agarwal, B., Michan, S., Puchowicz, M.A., Nakamaru-Ogiso, E., and Baur, J.A. (2015). Increasing NAD synthesis in muscle via nicotinamide phosphoribosyltransferase is not sufficient to promote oxidative metabolism. *J. Biol. Chem.* 290, 1546–1558.
- Gomes, A.P., Price, N.L., Ling, A.J., Moslehi, J.J., Montgomery, M.K., Rajman, L., White, J.P., Teodoro, J.S., Wrann, C.D., Hubbard, B.P., et al. (2013). Declining NAD⁺ induces a pseudohypoxic state disrupting nuclear-mitochondrial communication during aging. *Cell* 155, 1624–1638.
- Groen, B.B., Hamer, H.M., Snijders, T., van Kranenburg, J., Frijns, D., Vink, H., and van Loon, L.J. (2014). Skeletal muscle capillary density and microvascular function are compromised with aging and type 2 diabetes. *J. Appl. Physiol.* 116, 998–1005.
- Guarani, V., Deflorian, G., Franco, C.A., Krüger, M., Phng, L.K., Bentley, K., Toussaint, L., Dequiedt, F., Mostoslavsky, R., Schmidt, M.H., et al. (2011). Acetylation-dependent regulation of endothelial Notch signalling by the SIRT1 deacetylase. *Nature* 473, 234–238.
- Guarente, L. (2013). Calorie restriction and sirtuins revisited. *Genes Dev.* 27, 2072–2085.
- Haigis, M.C., and Sinclair, D.A. (2010). Mammalian sirtuins: biological insights and disease relevance. *Annu. Rev. Pathol.* 5, 253–295.
- Harman, D. (1956). Aging: a theory based on free radical and radiation chemistry. *J. Gerontol.* 11, 298–300.
- Hine, C., and Mitchell, J.R. (2015). Calorie restriction and methionine restriction in control of endogenous hydrogen sulfide production by the transsulfuration pathway. *Exp. Gerontol.* 68, 26–32.
- Hood, D.A. (2001). Invited review: contractile activity-induced mitochondrial biogenesis in skeletal muscle. *J. Appl. Physiol.* 90, 1137–1157.
- Hu, M.Z., Zhou, B., Mao, H.Y., Sheng, Q., Du, B., Chen, J.L., Pang, Q.F., and Ji, Y. (2016). Exogenous hydrogen sulfide postconditioning protects isolated rat hearts from ischemia/reperfusion injury through Sirt1/PGC-1 α signaling pathway. *Int. Heart J.* 57, 477–482.
- Hubbard, B.P., Gomes, A.P., Dai, H., Li, J., Case, A.W., Considine, T., Riera, T.V., Lee, J.E., E, S.Y., Lamming, D.W., et al. (2013). Evidence for a common mechanism of SIRT1 regulation by allosteric activators. *Science* 339, 1216–1219.
- Hughes-Large, J.M., Pang, D.K., Robson, D.L., Chan, P., Toma, J., and Borradaile, N.M. (2014). Niacin receptor activation improves human microvascular endothelial cell angiogenic function during lipotoxicity. *Atherosclerosis* 237, 696–704.
- Kanfi, Y., Naiman, S., Amir, G., Peshti, V., Zinman, G., Nahum, L., Bar-Joseph, Z., and Cohen, H.Y. (2012). The sirtuin SIRT6 regulates lifespan in male mice. *Nature* 483, 218–221.
- Korff, T., and Augustin, H.G. (1998). Integration of endothelial cells in multicellular spheroids prevents apoptosis and induces differentiation. *J. Cell Biol.* 143, 1341–1352.
- Kuznetsov, A.V., Veksler, V., Gellerich, F.N., Saks, V., Margreiter, R., and Kunz, W.S. (2008). Analysis of mitochondrial function in situ in permeabilized muscle fibers, tissues and cells. *Nat. Protoc.* 3, 965–976.
- Lagouge, M., Argmann, C., Gerhart-Hines, Z., Meziane, H., Lerin, C., Daussin, F., Messadeq, N., Milne, J., Lambert, P., Elliott, P., et al. (2006). Resveratrol improves mitochondrial function and protects against metabolic disease by activating SIRT1 and PGC-1 α . *Cell* 127, 1109–1122.

- Le Couteur, D.G., and Lakatta, E.G. (2010). A vascular theory of aging. *J. Gerontol. A Biol. Sci. Med. Sci.* *65*, 1025–1027.
- Li, S., Czubryt, M.P., McAnally, J., Bassel-Duby, R., Richardson, J.A., Wiebel, F.F., Nordheim, A., and Olson, E.N. (2005). Requirement for serum response factor for skeletal muscle growth and maturation revealed by tissue-specific gene deletion in mice. *Proc. Natl. Acad. Sci. USA* *102*, 1082–1087.
- Li, J., Bonkowski, M.S., Moniot, S., Zhang, D., Hubbard, B.P., Ling, A.J., Rajman, L.A., Qin, B., Lou, Z., Gorbunova, V., et al. (2017). A conserved NAD⁺ binding pocket that regulates protein-protein interactions during aging. *Science* *355*, 1312–1317.
- Limbourg, A., Korff, T., Napp, L.C., Schaper, W., Drexler, H., and Limbourg, F.P. (2009). Evaluation of postnatal arteriogenesis and angiogenesis in a mouse model of hind-limb ischemia. *Nat. Protoc.* *4*, 1737–1746.
- Lin, J., Wu, H., Tarr, P.T., Zhang, C.Y., Wu, Z., Boss, O., Michael, L.F., Puigserver, P., Isotani, E., Olson, E.N., et al. (2002). Transcriptional co-activator PGC-1 alpha drives the formation of slow-twitch muscle fibres. *Nature* *418*, 797–801.
- Longchamp, A., Mirabella, T., Arduini, A., MacArthur, M.R., Das, A., Treviño-Villarreal, J.H., Hine, C., Ben-Sahra, I., Knudsen, N.H., Brace, L.E., et al. (2018). Amino Acid Restriction Triggers Angiogenesis via GCN2/ATF4 Regulation of VEGF and H₂S Production. *Cell* *173*, this issue, ■■■■-■■■■.
- Mattagajasingh, I., Kim, C.S., Naqvi, A., Yamamori, T., Hoffman, T.A., Jung, S.B., DeRicco, J., Kasuno, K., and Irani, K. (2007). SIRT1 promotes endothelium-dependent vascular relaxation by activating endothelial nitric oxide synthase. *Proc. Natl. Acad. Sci. USA* *104*, 14855–14860.
- Mersmann, N., Tkachev, D., Jelinek, R., Röth, P.T., Möbius, W., Ruhwedel, T., Rühle, S., Weber-Fahr, W., Sartorius, A., and Klugmann, M. (2011). Aspartoacylase-lacZ knockin mice: an engineered model of Canavan disease. *PLoS ONE* *6*, e20336.
- Miller, D.L., and Roth, M.B. (2007). Hydrogen sulfide increases thermotolerance and lifespan in *Caenorhabditis elegans*. *Proc. Natl. Acad. Sci. USA* *104*, 20618–20622.
- Mills, K.F., Yoshida, S., Stein, L.R., Grozio, A., Kubota, S., Sasaki, Y., Redpath, P., Migaud, M.E., Apte, R.S., Uchida, K., et al. (2016). Long-term administration of nicotinamide mononucleotide mitigates age-associated physiological decline in mice. *Cell Metab.* *24*, 795–806.
- Morscher, S., Driessen, W.H., Claussen, J., and Burton, N.C. (2014). Semi-quantitative Multispectral Optoacoustic Tomography (MSOT) for volumetric PK imaging of gastric emptying. *Photoacoustics* *2*, 103–110.
- Mouchiroud, L., Houtkooper, R.H., and Auwerx, J. (2013). NAD⁺ metabolism: a therapeutic target for age-related metabolic disease. *Crit. Rev. Biochem. Mol. Biol.* *48*, 397–408.
- Narkar, V.A., Downes, M., Yu, R.T., Emblar, E., Wang, Y.X., Banayo, E., Mihaylova, M.M., Nelson, M.C., Zou, Y., Jugulion, H., et al. (2008). AMPK and PPAR-delta agonists are exercise mimetics. *Cell* *134*, 405–415.
- Nosedá, M., Chang, L., McLean, G., Grim, J.E., Clurman, B.E., Smith, L.L., and Karsan, A. (2004). Notch activation induces endothelial cell cycle arrest and participates in contact inhibition: role of p21Cip1 repression. *Mol. Cell. Biol.* *24*, 8813–8822.
- Olfert, I.M., Howlett, R.A., Tang, K., Dalton, N.D., Gu, Y., Peterson, K.L., Wagner, P.D., and Breen, E.C. (2009). Muscle-specific VEGF deficiency greatly reduces exercise endurance in mice. *J. Physiol.* *587*, 1755–1767.
- Oommen, S., Gupta, S.K., and Vlahakis, N.E. (2011). Vascular endothelial growth factor A (VEGF-A) induces endothelial and cancer cell migration through direct binding to integrin alpha9beta1: identification of a specific alpha9beta1 binding site. *J. Biol. Chem.* *286*, 1083–1092.
- Ota, H., Akishita, M., Eto, M., Iijima, K., Kaneki, M., and Ouchi, Y. (2007). Sirt1 modulates premature senescence-like phenotype in human endothelial cells. *J. Mol. Cell. Cardiol.* *43*, 571–579.
- Pearson, K.J., Baur, J.A., Lewis, K.N., Peshkin, L., Price, N.L., Labinskyy, N., Swindell, W.R., Kamara, D., Minor, R.K., Perez, E., et al. (2008). Resveratrol delays age-related deterioration and mimics transcriptional aspects of dietary restriction without extending life span. *Cell Metab.* *8*, 157–168.
- Pette, D., and Staron, R.S. (2000). Myosin isoforms, muscle fiber types, and transitions. *Microsc. Res. Tech.* *50*, 500–509.
- Potente, M., Ghaeni, L., Baldessari, D., Mostoslavsky, R., Rossig, L., Dequiedt, F., Haendeler, J., Mione, M., Dejana, E., Alt, F.W., et al. (2007). SIRT1 controls endothelial angiogenic functions during vascular growth. *Genes Dev.* *21*, 2644–2658.
- Price, N.L., Gomes, A.P., Ling, A.J., Duarte, F.V., Martin-Montalvo, A., North, B.J., Agarwal, B., Ye, L., Ramadori, G., Teodoro, J.S., et al. (2012). SIRT1 is required for AMPK activation and the beneficial effects of resveratrol on mitochondrial function. *Cell Metab.* *15*, 675–690.
- Prior, S.J., Ryan, A.S., Blumenthal, J.B., Watson, J.M., Katzell, L.I., and Goldberg, A.P. (2016). Sarcopenia is associated with lower skeletal muscle capillarization and exercise capacity in older adults. *J. Gerontol. A Biol. Sci. Med. Sci.* *71*, 1096–1101.
- Ramsey, K.M., Mills, K.F., Satoh, A., and Imai, S. (2008). Age-associated loss of Sirt1-mediated enhancement of glucose-stimulated insulin secretion in beta cell-specific Sirt1-overexpressing (BESTO) mice. *Aging Cell* *7*, 78–88.
- Respress, J.L., and Wehrens, X.H. (2010). Transthoracic echocardiography in mice. *J. Vis. Exp.* (39), 1738.
- Rose, P., Dymock, B.W., and Moore, P.K. (2015). GYY4137, a novel water-soluble, H₂S-releasing molecule. *Methods Enzymol.* *554*, 143–167.
- Ross, J.M. (2011). Visualization of mitochondrial respiratory function using cytochrome c oxidase/succinate dehydrogenase (COX/SDH) double-labeling histochemistry. *J. Vis. Exp.* (57), 3266.
- Ryan, N.A., Zwetsloot, K.A., Westerkamp, L.M., Hickner, R.C., Pofahl, W.E., and Gavin, T.P. (2006). Lower skeletal muscle capillarization and VEGF expression in aged vs. young men. *J. Appl. Physiol.* *100*, 178–185.
- Salminen, A., Kaamiranta, K., and Kauppinen, A. (2013). Crosstalk between oxidative stress and SIRT1: impact on the aging process. *Int. J. Mol. Sci.* *14*, 3834–3859.
- Satoh, A., Brace, C.S., Rensing, N., Cliften, P., Wozniak, D.F., Herzog, E.D., Yamada, K.A., and Imai, S. (2013). Sirt1 extends life span and delays aging in mice through the regulation of Nk2 homeobox 1 in the DMH and LH. *Cell Metab.* *18*, 416–430.
- Sinclair, D.A., and Guarente, L. (2014). Small-molecule allosteric activators of sirtuins. *Annu. Rev. Pharmacol. Toxicol.* *54*, 363–380.
- Suo, R., Zhao, Z.Z., Tang, Z.H., Ren, Z., Liu, X., Liu, L.S., Wang, Z., Tang, C.K., Wei, D.H., and Jiang, Z.S. (2013). Hydrogen sulfide prevents H₂O₂-induced senescence in human umbilical vein endothelial cells through SIRT1 activation. *Mol. Med. Rep.* *7*, 1865–1870.
- Turner, N., Hariharan, K., TidAng, J., Frangioudakis, G., Beale, S.M., Wright, L.E., Zeng, X.Y., Leslie, S.J., Li, J.Y., Kraegen, E.W., et al. (2009). Enhancement of muscle mitochondrial oxidative capacity and alterations in insulin action are lipid species dependent: potent tissue-specific effects of medium-chain fatty acids. *Diabetes* *58*, 2547–2554.
- Uddin, G.M., Youngson, N.A., Sinclair, D.A., and Morris, M.J. (2016). Head to head comparison of short-term treatment with the NAD(+) precursor nicotinamide mononucleotide (NMN) and 6 weeks of exercise in obese female mice. *Front. Pharmacol.* *7*, 258.
- Ungvari, Z., Bagi, Z., Feher, A., Recchia, F.A., Sonntag, W.E., Pearson, K., de Cabo, R., and Csizsar, A. (2010). Resveratrol confers endothelial protection via activation of the antioxidant transcription factor Nrf2. *Am. J. Physiol. Heart Circ. Physiol.* *299*, H18–H24.
- van Beijnum, J.R., Rousch, M., Castermans, K., van der Linden, E., and Griffioen, A.W. (2008). Isolation of endothelial cells from fresh tissues. *Nat. Protoc.* *3*, 1085–1091.
- Wang, H., Listrat, A., Meunier, B., Gueugneau, M., Coudy-Gandilhon, C., Combarret, L., Taillandier, D., Polge, C., Attaix, D., Lethias, C., et al. (2014). Apoptosis in capillary endothelial cells in ageing skeletal muscle. *Aging Cell* *13*, 254–262.
- Wang, X., Lockhart, S.M., Rathjen, T., Albadawi, H., Sorensen, D., O'Neill, B.T., Dwivedi, N., Preil, S.R., Beck, H.C., Dunwoodie, S.L., et al. (2016). Insulin downregulates the transcriptional coregulator CITED2, an inhibitor of proangiogenic function in endothelial cells. *Diabetes* *65*, 3680–3690.

- Wei, T., Huang, G., Gao, J., Huang, C., Sun, M., Wu, J., Bu, J., and Shen, W. (2017). Sirtuin 3 deficiency accelerates hypertensive cardiac remodeling by impairing angiogenesis. *J. Am. Heart Assoc.* *6*, e006114.
- Wu, D., Hu, Q., Liu, X., Pan, L., Xiong, Q., and Zhu, Y.Z. (2015). Hydrogen sulfide protects against apoptosis under oxidative stress through SIRT1 pathway in H9c2 cardiomyocytes. *Nitric Oxide* *46*, 204–212.
- Yoshino, J., Mills, K.F., Yoon, M.J., and Imai, S. (2011). Nicotinamide mononucleotide, a key NAD(+) intermediate, treats the pathophysiology of diet- and age-induced diabetes in mice. *Cell Metab.* *14*, 528–536.
- Zhang, Y., Jiang, G., Sauler, M., and Lee, P.J. (2013). Lung endothelial HO-1 targeting in vivo using lentiviral miRNA regulates apoptosis and autophagy during oxidant injury. *FASEB J.* *27*, 4041–4058.
- Zhang, H., Ryu, D., Wu, Y., Gariani, K., Wang, X., Luan, P., D'Amico, D., Ropelle, E.R., Lutolf, M.P., Aebersold, R., et al. (2016). NAD⁺ repletion improves mitochondrial and stem cell function and enhances life span in mice. *Science* *352*, 1436–1443.
- Zheng, M., Qiao, W., Cui, J., Liu, L., Liu, H., Wang, Z., and Yan, C. (2014). Hydrogen sulfide delays nicotinamide-induced premature senescence via up-regulation of SIRT1 in human umbilical vein endothelial cells. *Mol. Cell. Biochem.* *393*, 59–67.
- Zu, Y., Liu, L., Lee, M.Y., Xu, C., Liang, Y., Man, R.Y., Vanhoutte, P.M., and Wang, Y. (2010). SIRT1 promotes proliferation and prevents senescence through targeting LKB1 in primary porcine aortic endothelial cells. *Circ. Res.* *106*, 1384–1393.

STAR★METHODS

KEY RESOURCES TABLE

REAGENT or RESOURCE	SOURCE	IDENTIFIER
Antibodies		
Anti-SIRT1	Sigma-Aldrich	Cat#HPA006295
Anti-SIRT1(Sir2)	Merck Millipore	Cat#07-131
SirT3 (D22A3) Rabbit	Cell Signaling Technology	Cat#5490
SIRT6 (6C9-D10-D3)	Santa Cruz Biotech	Cat#517556
eNOS	Cell Signaling Technology	Cat#9572
Cleaved Notch1 (Val1744) (D3B8) Rabbit	Cell Signaling Technology	Cat#4147
Total OXPHOS Rodent WB Antibody Cocktail	Abcam	Cat#110413
Anti-PGC-1 α Mouse (4C1.3)	Merck Millipore	Cat#ST1202
Pan-Actin	Cell Signaling Technology	Cat#4968
Monoclonal anti- α -tubulin	Sigma-Aldrich	Cat#T8203
14-3-3 (pan)	Cell Signaling Technology	Cat#8312
GAPDH (G-9)	Santa Cruz Biotech	Cat#sc-365062
Anti-CD31 (RM0032-1D12)	Abcam	Cat# ab56299
Anti-Laminin	Sigma-Aldrich	Cat#L9393
Anti-GFP	Abcam	Cat#ab6556
Anti-VEGFA	Abcam	Cat#ab46154
Phospho-VEGF Receptor 2 (Tyr1175) (19A10) Rb	Cell Signaling Technology	Cat#2478
Anti-VEGF Receptor 2	Abcam	Cat#ab39256
CD31-APC, mouse (clone: 390)	Miltenyl Biotec	Cat#130-102-571
APC anti-mouse CD31 (clone: MEC 13.3)	Biologend	Cat#102510
Alexa Fluor 488 Goat anti-rat IgG (H+L)	Life Technologies	Cat#A11006
Alexa Fluor 594 Goat anti-rabbit (H+L)	Life Technologies	Cat#A11012
Alexa Fluor 488 Goat anti-rabbit IgG (H+L)	Life Technologies	Cat#R37116
Alexa Fluor 594 Goat anti-rat (H+L)	Life Technologies	Cat#A11007
Bacterial and Virus Strains		
GFP Adenovirus	Abmgood	Cat#000541A
SIRT1 Adenovirus (Human)	Abmgood	Cat#131079A
Chemicals, Peptides, and Recombinant Proteins		
Rodent Chow Diet	LabDiet	Cat#5053
4-Hydroxytamoxifen	Sigma-Aldrich	Cat#H6278
Nicotinamide mononucleotide	Bontac Bio-Engineering, China	N/A
Sodium hydrosulfide	Sigma-Aldrich	Cat#161527
GY4137	Cayman Chemical	Cat#13345
DAPT (N-[N-(3,5-Difluorophenacetyl)-L-alanyl]-S-phenylglycine t-butyl ester)	Sigma-Aldrich	Cat#13197
SU5416	Sigma-Aldrich	Cat#13342
Axitinib	Selleck Chemical	Cat#S1005
Hydrogen peroxide, 35% stabilized	VWR	Cat#BDH7814-3
Triton X-100	Sigma-Aldrich	Cat#X100
Oligomycin A	Sigma-Aldrich	Cat#75351
TRIzol Reagent	Life Technologies	Cat#15596018
Collagenase/Dispase	Sigma-Aldrich	Cat#11097113001
DnaseI	Sigma-Aldrich	Cat#10104159001

(Continued on next page)

Continued

REAGENT or RESOURCE	SOURCE	IDENTIFIER
Methocel (viscosity: 4000 cps)	Sigma-Aldrich	Cat#M0512
BS1 lectin-FITC	Sigma-Aldrich	Cat#9381
Fetal Bovine Serum (FBS)	Life Technologies	Cat#10099141
Penicillin/Streptomycin (10,000 U/mL)	Life Technologies	Cat#15140122
Cytochrome c Oxidase from bovine heart	Sigma-Aldrich	Cat#C-5499
Basic Fibroblast Growth Factor (bFGF)	Corning	Cat#354060
VEGF Recombinant Human Protein	Life Technologies	Cat#PHC9394
VEGF Recombinant Mouse Protein	Life Technologies	Cat#PMG0114
FGF Recombinant Mouse Protein	Life Technologies	Cat#PMG0034
Recombinant mouse Dll4 protein	R&D Systems	Cat#1389-D4-050
Cytochrome c from equine heart	Sigma-Aldrich	Cat#C2506
Catalase from bovine liver	Sigma-Aldrich	Cat#C60629
3,3'-diaminobenzidine (DAB)	Sigma-Aldrich	Cat#D12384
Collagen, Type I, Rat tail	Merck Millipore	Cat#08-115
Cultrex® Reduced Growth Factor Basement Membrane Matrix	Trevigen	Cat#3533-001-02
Dharmafect 4 Transfection Reagent	Dharmacon	Cat#T-2004-03
Polybrene	Sigma-Aldrich	Cat#H9268
Puromycin Sulfate	Sigma-Aldrich	Cat#P8833
FuGENE HD transfection reagent	Promega	Cat#E2311
<i>Ascl</i>	New England Biolabs	Cat#R0558L
EcoRI	New England Biolabs	Cat#R010L
Pierce 16% formaldehyde (w/v), methanol free	Life Technologies	Cat#28906
O.C.T. Embedding Compound	Grale HDS	Cat#4583SD
BlockAid blocking solution	Life Technologies	Cat#B10710
Fluoroshield mounting medium with DAPI	Sigma-Aldrich	Cat#F6057
DPX mounting medium	Grale HDS	Cat#1.00579.0500
iScript Reverse Transcription Supermix	Biorad	Cat#170-8840
LightCycler 48 SYBR Green I Mastermix	Roche	Cat#04707516001
Critical Commercial Assays		
Creatinine (urinary) Colorimetric Assay Kit	Cayman Chemical	Cat#500701
Mouse VEGF-A ELISA kit	RayBiotech	Cat#ELM-VEGF-1
NAD-NADH Glo Assay Kit	Promega	Cat#G9071
Block-iT Pol II miR RNAi Expression Vector Kit	Life Technologies	Cat#K4936-00
TUNEL Assay kit (<i>in situ</i> BrDU-Red DNA Fragmentation)	Abcam	Cat#ab66110
Annexin V-FITC apoptosis detection kit	Life Technologies	Cat#BMS500FI
EasySep Mouse APC Positive Selection Kit	Stem Cell Technologies	Cat#18452
Lenti-X qRT-PCR titration kit	Takara Biosciences	Cat#631235
Experimental Models: Cell Lines		
Human Umbilical Vein Endothelial Cells	Lonza	Cat #CC2519A
Human Aortic Endothelial Cells	Lonza	Cat#CC2535
C2C12	Sinclair Lab	N/A
HEK293T	Sinclair Lab	N/A
Experimental Models: Organisms/Strains		
Mouse: C57BL/6J	ABR (AU), ARC (AU), NIA (US)	N/A
Mouse: C57BL/6J SIRT1-iKO	Housed in HCCM Animal Facility	Price et al., 2012
Mouse: C57BL/6J SIRT1-Tg	Housed in HCCM Animal Facility	Firestein et al., 2008

(Continued on next page)

Continued

REAGENT or RESOURCE	SOURCE	IDENTIFIER
Mouse: C57BL/6J <i>SIRT1</i> ^{STOP}	Housed in HCCM Animal Facility	Firestein et al., 2008
Mouse: <i>Tie2-Cre</i> (B6.Cg-Tg(Tek-cre)12Flv/J)	The Jackson Laboratory	JAX:004128
Mouse: <i>SIRT1</i> ^{flf} (B6.129-Sirt1 ^{tm3Fwa} /DsinJ)	The Jackson Laboratory	JAX:029603
Mouse: <i>mT-STOP</i> ^{flf} -GFP (B6.129(Cg)- <i>Gt(ROSA)26Sor</i> ^{tm4(ACTB-tdTomato,-EGFP)^{Luo}/J})	The Jackson Laboratory	JAX:007676
Mouse: C57BL/6J <i>Myog-Cre</i>	Gift from Dr. Eric N. Olson, UT Southwestern TX	Li et al., 2005
Mouse: C57BL/6J <i>MCK-PGC-1α</i>	Gift from Dr. Bruce Spiegelman, Dana Farber Cancer Center MA	Lin et al., 2002
Oligonucleotides		
Sir2A6860	CATGTAATCTCAACCTTGAG	N/A
Sir2A6171	GCCCATTAAGCAGTATGTG	N/A
miRNA Oligos	Table S1	N/A
RTqPCR Primers	Table S2	N/A
ON-TARGETplus Non-targeting Pool siRNA	Dharmacon	Cat#DHA-D-001810-10-05
SMARTpool ON-TARGETplus Human SIRT1 siRNA	Dharmacon	Cat#L-003540-00-0005
SMARTpool ON-TARGETplus Human SIRT3 siRNA	Dharmacon	Cat#L-004827-01-0005
SMARTpool ON-TARGETplus Human SIRT6 siRNA	Dharmacon	Cat#L-013306-00-0005
Recombinant DNA		
pLKO.1 puro plasmid	Gift from Dr. Bob Weinberg	Addgene #8453
pLKO.1 Scr shRNA plasmid	Generated in house by Dr. Eric Bell (MIT)	N/A
pLKO.1 SIRT1 shRNA plasmid	Generated in house by Dr. Eric Bell (MIT)	N/A
psPAX2	Gift from Dr. Didier Trono	Addgene #12260
pMD2.G	Gift from Dr. Didier Trono	Addgene #12259
pcDNA6.2-GW/EmGFP-miR plasmid	Life Technologies	Cat#K4936-00
pcDNA6.2-GW/EmGFP-miR negative control plasmid	Life Technologies	Cat#K4936-00
Lenti-VE-Cad miRNA plasmid	Gift from Dr. Patty J. Lee (Yale University)	Zhang et al., 2013
Software and Algorithms		
Adobe Creative Suite	Adobe	https://www.adobe.com
FlowJo v10	FlowJo	https://www.flowjo.com/
GraphPad Prism v7	GraphPad Software	https://www.graphpad.com/scientific-software/prism/
Fiji	NIH	http://imagej.net/Fiji/Downloads
BLOCK-iT RNAi designer	Invitrogen	https://rnaidesigner.thermofisher.com/rnaexpress/
Other		
EGM-2 bulletkit	Lonza	Cat#CC-3162
DMEM, high glucose, GlutaMAX Supplement	Life Technologies	Cat#10566-016
Opti-MEM/Reduced Serum Medium	Life Technologies	Cat#31985-070
4-15% Criterion TGX Precast Protein Gel	Biorad	http://www.bio-rad.com
Vevo Micromarker Non-targeted contrast agent	Fujifilm VisualSonics	Cat#VS-11913
Vevo 2100 System	VisualSonics	https://www.visualsonics.com
MSOT inVision 256-TF Imaging System	iThera Medical GmbH	http://www.ithera-medical.com
Oxyman/CLAMS System	Columbus Instruments	http://www.colinst.com
EchoMRI-900	EchoMRI	http://www.echomri.com

(Continued on next page)

Continued

REAGENT or RESOURCE	SOURCE	IDENTIFIER
96-well plates, polystyrene round bottom, non-treated, well volume 330 μ L, sterile	Sigma-Aldrich	Cat#CLS3795
FluoroBlok transwell (8 μ m pore diameter)	Corning	Cat#351152
Cryomolds 15x15x5 mm intermediate	Grale HDS	Cat#4566
Menzel Slides Superfrost Plus 25x75mm	Grale HDS	Cat#SF41296SP
HD Scientific Coverslips	Grale HDS	Cat#LD2250
Cryostat	Leica Biosystems	N/A
● gentleMACS Octo Dissociator with Heaters	Miltenyl Biotech	Cat#130-096-427
FACSCanto II Analyzer	BD Biosciences	http://www.bdbiosciences.com
BD LSR II	BD Biosciences	http://www.bdbiosciences.com
Seahorse XF96 analyzer	Agilent Technologies	https://www.agilent.com
1050-RM Exer 3/6 Open Treadmill	Columbus Instruments	http://www.colinst.com
Clark-type electrode	Rank Brothers	http://www.rankbrothers.co.uk
Accu-Check Performa Blood Glucose Meter	Roche	https://www.roche.com
Accutrend Plus System	Roche	https://www.roche.com

CONTACT FOR REAGENT AND RESOURCES SHARING

Further information and requests for resources and reagents should be directed to and will be fulfilled by the Lead Contact, Dr. David A. Sinclair (david_sinclair@hms.harvard.edu).

EXPERIMENTAL MODEL AND SUBJECT DETAILS

Animals

All experiments were performed according to procedures approved by UNSW Animal Care and Ethics Committee (UNSW, Australia), MIT's Committee on Animal Care (MIT, MA) and Institutional Animal Care and Use Committees (Harvard Medical School, MA). Mice were fed standard chow and housed under a 12 hr light/12 hr dark cycle.

The EC specificity of Tie2 promoter was determined by crossing a *Tie2-Cre* mouse to a reporter mouse (*mT-STOP^{flf}-GFP*). *mT-STOP^{flf}-GFP* mouse expresses membrane-targeted tandem dimer Tomato protein (TOMATO) ubiquitously. When crossed to *Tie2-Cre* mouse (*Tie2-Cre-GFP*) green fluorescent protein (EGFP) is expressed. *Tie2-Cre* mouse was crossed to *SIRT1^{flf}* or *SIRT1^{STOP}* mouse to generate ESKO (*Tie2-Cre;SIRT1^{flf}*) (Cheng et al., 2003; Potente et al., 2007) or ESTO (*Tie2-Cre;SIRT1^{STOP}*) mouse, respectively. *Myog-Cre* was crossed to *SIRT1^{flf}* mouse to generate MSKO mouse. *MCK-PGC-1 α* mouse was crossed to ESKO or MSKO mouse where required.

SIRT1-iKO mice were fed tamoxifen (360 mg/kg) diet for five weeks to elicit whole-body SIRT1 exon 4 excision as described previously (Price et al., 2012). In all cases, otherwise indicated, animals were administered NMN (400 mg/kg/day), NaHS (20 mg/kg/day) and/or GYY4137 (20 mg/kg/day) (Rose et al., 2015) via drinking water. NMN stock was changed twice per week and NaHS/GYY4137 was supplemented daily.

Cells

C2C12 and HEK293T cells were grown in DMEM supplemented with 10% FBS and 1% Penicillin/Streptomycin (Pen/Strep) at 37°C with 5% CO₂. ECs (HUVEC, HAEC and MLEC) were cultured in EGM-2 media at 37°C with 3% O₂ and 5% CO₂.

METHOD DETAILS

Endurance testing of mice

Mice were acclimatized to the treadmill system for 3 days prior to endurance testing by running at 10-15 m/min for 20 min. In low intensity endurance testing, the speed started at 5 m/min for 5 min, and then the speed was increased by 1 every minute until 21 m/min and kept constant. In high intensity endurance testing, the speed started at 13 m/min for 5 min at 5° inclination, and then the speed was increased by 1 every minute until 20 m/min and kept constant for 20 min. Every 20 min, the speed was increased by 5 m/min and held constant for 20 min. In both tests, mice were run until exhaustion. Mice were considered exhausted when they sat on the shocker plate for more than 10 s without attempting to reinitiate running.

Exercise training of mice

Mice were acclimatized to the treadmill system for 3 days prior to the start of exercise training by running at 10 m/min for 20 min. The animals that were successfully acclimated were then trained at 15–20 m/min at 5° inclination for 30 minutes once daily for 30 days. Mice receiving treatment were given NMN (500 mg/kg/day) and/or axitinib (30 mg/kg/day) throughout the course of exercise training regimen. NMN given via drinking water was changed every 3 days and axitinib (Escudier and Gore, 2011) given via food was changed daily. The exhaustive exercise capacity of the mice was tested at the end of training.

Blood glucose, lactate and VEGF

Mice were fasted for 6 hr and blood glucose levels were measured by tail bleed using a commercially available glucose meter. Blood lactate was measured before and immediately after treadmill exercise (30 min at 15 m/min) by tail bleed using a commercially available lactate meter. Serum VEGF was measured using a commercially available ELISA kit or by Eve Technologies, Canada.

Urine creatinine

Urine was collected from mice after a 2 hr fast and analyzed for creatinine levels using a colorimetric assay kit.

Rotarod test

Motor coordination was assessed using the rotarod test as previously described (Mersmann et al., 2011). In short, mice were acclimatized to a rotarod for 3 days in three trials lasting 2 min each at a constant speed of 5 rpm. On the 4th day, the animals were subjected to three trials on the accelerating roller (4 - 40 rpm in 4 min) and the time that the mice remained was recorded.

Hindlimb ischemia

The effect of NMN in ischemia-induced vessel formation was assessed in a murine model of hindlimb ischemia using 8-month old SIRT1-iKO and WT mice according to the published protocol (Limbourg et al., 2009). Treatment of animals with NMN (500 mg/kg/day) via drinking water started one week prior to femoral ligation and was continued until the end of the experiment. The blood flow in the ischemic limb was measured using contrast-enhanced ultrasound imaging, 20 days after the surgery.

Contrast-enhanced ultrasound (CEU)

Mice were anesthetized with isoflurane (1.5%–2%, 500 mL O₂/min), hindlimbs were shaved using depilatory cream and a 27-gauge catheter was placed into each mouse's tail and kept in place with surgical tape. Each mouse was placed in a supine position on a platform heated to 38°C with each paw taped to a surface electrode to monitor ECG, heart rate, and respiratory rate. CEU was performed using Vevo 2100 system at an imaging frequency of 18 MHz. The probe was placed on the medial side of the leg to image the lower hindlimb in a sagittal plane. A bolus injection of microbubbles (contrast reagents) were injected through the tail vein catheter according to the manufacturer's instructions. A cine loop was recorded at a frame rate of 20 frames/s for a total of 1,000 frames. Curve fit analysis was used to measure echo power over time. The difference in maximum and minimum video intensity was determined as the peak enhancement (Baltgalvis et al., 2014).

Cardiac ultrasound

Parasternal short-axis M-mode images were acquired using the Vevo 2100 system as previously described (Respress and Wehrens, 2010). Mice were anesthetized with 1%–2% isoflurane, and heart rate was measured between 450 and 500 beats/min.

Photoacoustic imaging

Mice were anesthetized with isoflurane (1.5%–2%, 500 mL O₂/min), and body portion below chest area was shaved using depilatory cream. The animals were then placed horizontally in the imaging chamber of MSOT inVision 256-TF small animal imaging system and three-dimensional scanning of the lower portion was performed as per manufacturer's protocol (Morscher et al., 2014). Briefly, a tunable optical parametric oscillator (OPO) pumped by an Nd:YAG laser provided excitation pulses with a duration of 9 ns at wavelengths from 680 nm to 980 nm at a repetition rate of 10 Hz with a wavelength tuning speed of 10 ms and a peak pulse energy of 100 mJ at 730 nm. Ten arms of a fiber bundle provided even illumination of a ring-shaped light strip of approx. 8 mm width. For ultrasound detection, 256 toroidally focused ultrasound transducers with a center frequency of 5 MHz (60% bandwidth), organized in a concave array of 270° angular coverage and a radius of curvature of 4 cm, were used.

Metabolic measurements and body composition

Metabolic chambers were used to perform whole-body measurements of metabolic function. Following acclimatization to the metabolic chambers, individually housed mice were monitored continuously over 48 hr to determine oxygen consumption, carbon dioxide production, respiratory exchange ratio, energy expenditure, food intake, water intake and activity. Body composition (fat mass, lean mass, and total body water) was measured by EchoMRI.

Permeabilized fiber respiration

Permeabilized fibers were prepared and mitochondrial function was analyzed according to published protocols with some modifications (Kuznetsov et al., 2008). Briefly, soleus and extensor digitorum longus (EDL) muscles were dissected tendon-to-tendon into ice-cold isolation buffer A and fibers were prepared immediately. Fiber bundles (~3 mg wet weight) were treated with saponin (50 μg/mL) for 20 min at 4°C and subsequently washed in cold respiration medium B (0.5 mM EGTA, 3 mM MgCl₂·6H₂O, 20 mM taurine, 10 mM KH₂PO₄, 20 mM HEPES, 0.1% BSA, 15 mM potassium-lactobionate, 110 mM mannitol, 0.3 mM dithiothreitol, pH 7.1). Mitochondrial respiratory chain function was analyzed on a Clark-type electrode *in situ* in respiration medium B at 37°C with the sequential addition of glutamate (10 mM), malate (5 mM), ADP (2 mM), rotenone (0.5 μM), succinate (10 mM), antimycin A (5 μM), *N,N,N',N'*-tetramethyl-*p*-phenylenediamine dihydrochloride (0.5 mM TMPD) and ascorbate (2 mM), cytochrome *c* (10 μM). Fibers were recovered after polarography and results were expressed as nmoles of O₂/min/mg of tissue. Mitochondrial membrane integrity was verified by cytochrome *c* release test.

Enzyme activity assays

Quadriceps muscle was homogenized 1:19 (w/v) in 50 mM Tris-HCl, 1 mM EDTA, 0.1% Triton X-100, pH 7.4. The homogenates were subjected to three freeze-thaw cycles and centrifuged for 10 min at 7,000 × g at 4°C. Supernatants were used to determine the activity for citrate synthase (CS) and succinate dehydrogenase (SDH) as described previously (Turner et al., 2009). Cytochrome *c* oxidase staining of muscle sections was performed according to the published protocol (Ross, 2011). Briefly, 20 μm cryostat sections of quadriceps muscle were incubated with Cytochrome *c* (0.1 mM), catalase (2 μg/mL) and DAB (0.05%) in PBS for 40 min at 37°C. The slides were dehydrated through alcohol, cleared in xylene and then mounted with DPX. The slides were imaged using Aperio XT Slide Scanner.

NAD⁺ measurements

Levels of NAD⁺ in ECs and muscle homogenates were measured using commercially available kit. Alternatively, NAD⁺ levels in muscle and liver were measured by assay in-house developed method (Uddin et al., 2016). In brief, liver and gastrocnemius samples were homogenized in extraction buffer (10 mM Tris-HCl, 0.5% Triton X-100, 10 mM Nicotinamide, pH 7.4) and then centrifuged (12,000 × g for 5 min at 4°C), after which an aliquot of supernatant was taken for protein quantification. After phenol:chloroform:isoamylalcohol (25:24:1) and chloroform extractions the supernatant was separated in two aliquots. One was used to measure total NAD. The other aliquot was acidified with HCl, and then neutralized with NaOH on ice to quantify NAD⁺. Samples were mixed in a 96-well plate samples were mixed with alcohol dehydrogenase at room temperature. Total NADH and NAD⁺ were quantified using a plate reader.

Genotyping PCR analysis

Small piece of tail or tissue obtained from SIRT1-iKO and WT was incubated in 50 μL of alkaline lysis reagent (25 mM NaOH, 0.2 mM EDTA, pH 12) and incubated at 100°C for 1 hr. After cooling, 50 μL of neutralizing reagent (40 mM Tris-HCl, pH 5) was added and 2 μL of the supernatant was used for PCR to detect the excision of SIRT1 gene using the primers Sir2A6860 and Sir2A6171.

Primary mouse EC (MLEC) isolation

MLECs from lungs and muscles were isolated and purified according to published protocol (van Beijnum et al., 2008) with some modifications. Briefly, tissues were collected, weighed, rinsed with cold PBS, minced with sterile blades and then washed with DMEM media (10% FBS and 1% Pen/Strep). After adding 2.5 mL of digestion buffer (1 mg/mL Collagenase/Dispase, 0.1 mg/mL DnaseI in DMEM) per 100 mg of tissue, the mixture was incubated at 37°C for 20 min with shaking in a gentleMACS dissociator. The resulting suspension was then filtered through a 100-μ filter into an equal volume of washing/blocking buffer (20% FBS in PBS). The flow-through was spun at 300 × g for 5 min, supernatant discarded and the cells were suspended in 10 mL of washing/blocking buffer. The solution was filtered through 70-μ filter, spun again, resuspended in 2 mL RBC lysis buffer (155 mM NH₄Cl, 12 mM NaHCO₃ and 0.1 mM EDTA) and incubated for 5 min at room temperature. Immediately afterward, 10x volume of washing/blocking buffer was added and the solution was filtered through a 40-μ filter. The cells were collected by centrifugation, resuspended in Antibody Binding Buffer (2 mM EDTA, 1% FBS, 0.5% BSA and 2mM EDTA in PBS) and counted. MLECs were then isolated using CD31-APC antibody and EasySep mouse APC positive selection kit according to manufacturer's instructions. MLECs were cultured as described before.

Measurement of percent skeletal muscle ECs

Skeletal muscles from the hindlimbs were isolated, then digested with collagenase/dispase as described before and filtered through a 40-μ filter. The number of cells was counted and the cell suspension was incubated with APC-conjugated anti-mouse CD31 antibody for 20 min. Number of CD31⁺ ECs were measured and analyzed by flow cytometry.

RNA interference and viral infection

ECs were transfected with ON-Target^{plus} SMART pool siRNA reagents using Dharmafect 4 transfection reagent as per manufacturer's protocol. ON-TARGET^{plus} Non-Targeting pool siRNA (NT) was used as a negative control. SIRT1 silencing was also achieved

using pLKO.1 lentiviral plasmid mediated shRNA expression according to the published protocol (<http://www.addgene.org/tools/protocols/plko/>). Briefly, psPAX2, pMD2.G and lentiviral vector plasmids were co-transfected into 293T cells using FuGENE HD transfection reagent. At 48 hr post-transfection, virus was harvested and ECs were infected. pLKO.1 encoding a scrambled shRNA (Scr) was used as a negative control. ECs were infected with adenoviruses expressing human SIRT1 or GFP according to manufacturer's protocol. ECs were used for different angiogenesis assays, 24 hours post-transfection/infection.

Dll4 and VEGF stimulation of ECs

The ECs to be stimulated were serum-starved overnight and transferred to media containing VEGF (50 ng/mL) or Dll4-coated plates, and then incubated for indicated time. Dll4 coating was performed as described before (Guarani et al., 2011). Dll4 were reconstituted in PBS containing 0.1% bovine serum albumin (BSA). The culture dishes were coated with Dll4 (0.5 μg/mL) in 0.1% gelatin solution for 1 hr at 37°C. ECs were pre-incubated with NMN (0.5 mM) overnight prior to stimulation wherever indicated.

Construction of miRNA vectors and lentivirus production

The lentivirus plasmids expressing different miRNAs were constructed according to the published method (Zhang et al., 2013). Pre-miRNA sequences targeting mouse SIRT1 open reading frame (GenBank accession number NM_019812.3) were designed using the BLOCK-iT RNAi designer tool. Oligos corresponding to miRNAs (Table S1) were annealed and ligated into pcDNA6.2-GW/EmGFP-miR vector according to manufacturer's instructions. pcDNA6.2-GW/EmGFP-miR-neg control plasmid was used as a control. The fragments carrying EmGFP and miRNA sequences were amplified by polymerase chain reaction (PCR) using the primers: sense, 5'-AGGCGCGCCTGGCTAACTAGAGAAC-3', and antisense, 5'-GAATTCTATCTCGAGTGC GGC-3'. The amplified fragments were digested with *AscI* and *EcoRI*, and then inserted into the *AscI* and *EcoRI* sites of Lenti-VE-Cad miRNA plasmid to generate lentiviral plasmids expressing NT or SIRT1 miRNAs (#1-4). Lentiviral particles were produced as described before and concentrated in PBS by ultracentrifugation to $\sim 1 \times 10^{12}$ transducing units (TU)/mL. The lentiviral titer was measured using a qRT-PCR titration kit according to the manufacturer's instructions.

MLECs were infected with lentiviral particles at a multiplicity of infection (MOI) of 30. Lentiviral particles (1×10^{10} TU) were injected to animals via retro-orbital injection. Mice received two consecutive injections behind alternate eyes two days apart. 10 days post final injection; mice were assigned to different treatment groups. Cells/mice expressing SIRT1 miRNA #5 was generated by co-infecting equal titers of lentiviral particles carrying SIRT1 miRNA #1 and #4.

C2C12 Conditioned Media (CM)

C2C12 myoblasts transfected with adenovirus expressing PGC-1 α were differentiated in DMEM supplemented with 5% heat inactivated horse and then conditioned media (CM) was collected by replacing the differentiation medium with DMEM (1% FBS) medium for 48 hr.

Transwell migration assay

Chemotaxis assays were performed as described previously (Oommen et al., 2011). Primary murine lung endothelial cells (MLECs) were serum-starved overnight and then seeded ($2.5 - 5 \times 10^4$ cells) in the upper compartment of a transwell. C2C12 CM or DMEM was added to the bottom well to serve as chemo-attractant for MLECs. HUEVCs and HAECs were stimulated with EBM-2 media (0.2% FBS) containing VEGF (50 ng/mL) or FGF (50 ng/mL). NMN (0.5 mM) and/or NaHS (0.1 mM) were added to the chemo-attractant media wherever mentioned. ECs were allowed to migrate for 24 hr, after which cells were fixed, stained with DAPI and quantified by Fiji software. For each biological replicates (see figure legend) at least three random fields were photographed (@10X, Nikon Eclipse Ti).

TUBE FORMATION ASSAY

Formation of tube networks was assessed as described before (Borradaile and Pickering, 2009). ECs were seeded at 10,000 cells per well in a 24-well plate coated with 150 μL Cultrex reduced growth factor basement membrane matrix. The cells were simulated with C2C12 CM or EBM-2 medium containing VEGF (30 ng/mL) or FGF (30 ng/mL). NMN (0.5 mM) and NaHS (0.1 mM) were added to the media wherever mentioned. Following an 18 hr-incubation, resulting tube networks from each biological replicates (see figure legend) were analyzed in at least three random fields by light microscopy (@10X, Nikon Eclipse TiE). The number of branch points and total length of tubule networks were quantified by Fiji software (Angiogenesis Analyzer).

Spheroid assay

EC spheroids were generated as described previously (Korff and Augustin, 1998). Briefly, ECs (1000 cells per spheroid) were suspended in EGM-2 medium containing 20% methocel and seeded in non-adherent round-bottom 96-well plates. Under these conditions all suspended cells contributed to the formation of a single spheroid. The spheroids were harvested after 24 hr and embedded into 400 μL of 2.2 mg/mL collagen gels. Sprouting was initiated by adding 200 μL of C2C12 CM or EBM-2 medium containing VEGF (50 ng/mL). DMEM (1% FBS) or EBM-2 (BSA) was used as control for C2C12 CM or EBM-2 (VEGF), respectively. NMN (0.5 mM), NaHS (0.1 mM), DAPT (20 μM) or SU5416 (10 μM) were added to the media wherever mentioned. After 24 hr, spheroids

were photographed using phase-contrast microscopy (@10X, Nikon Eclipse Ti) and angiogenic capacity was quantified by measuring the sprout length that had grown out of each spheroid analyzing 8-10 spheroids per group. DAPT: γ -secretase inhibitor, SU5416: VEGFR2 inhibitor.

Aortic ring assay

Aortic ring assay was performed according to the published protocol (Baker et al., 2011). Briefly, thoracic aortas from mice were excised, cut into ~0.5 mm wide rings and serum starved overnight by incubating in Opti-MEM medium (1% Pen/Strep). Next day, each aortic ring was embedded in 50 μ L of 1 mg/mL collagen matrix in a 96-well plate and vessel sprouting was stimulated by supplementing with VEGF (30 ng/mL) or FGF (30 ng/mL) in 150 μ L of Opti-MEM culture containing FBS (2.5%). Control condition was minimal growth factors (2.5% FBS) with almost no sprouting because of low factor stimulation, as reported elsewhere (Baker et al., 2011). NMN (0.5 mM) or DAPT (20 μ M) were added to the media wherever mentioned. The media was replaced every two days. After incubating for 7 days, the resulting sprouts were stained with BS1 lectin-FITC and imaged using fluorescence microscope (@4X, Nikon A1). The number and total area of sprouts originating from aortic rings were quantified by Fiji software. Aortic rings were collected from at least 8 mice per experiment (see figure legend) and assay was performed using 4-5 technical replicates.

Wound scratch assay

ECs were cultured in a 24-well plate until forming a confluent monolayer and a scratch was made using a 200 μ L pipette tip. ECs were allowed to migrate \pm NaHS (0.1 mM) and \pm NMN (0.5 mM) in EGM-2 medium for 6 hr. Images were taken at the same location using a brightfield inverted microscope (Olympus 2467) every 2 hr. The area of gap closure was calculated using Fiji software.

Proliferation assay

ECs (0.1×10^5 cells) were seeded in a 48-well plate and incubated \pm NMN (0.5 mM) in EGM-2 medium for 48 hr. At the end of the incubation time, cell number was determined using flow cytometry.

Apoptosis assay

HUVECs were pretreated \pm NaHS (0.1 mM), \pm NMN (0.5 mM) for 6 hr, followed by exposure to H₂O₂ (0.6 mM) for another 4 hr. After treatments, the number of apoptotic cells was determined using Annexin V-FITC apoptosis detection kit as per manufacturer's instruction. Annexin-V and PI staining were detected with a flow cytometry. MLECs were serum starved overnight \pm NMN (0.5 mM) and the number of apoptotic cells was determined as above.

Seahorse analysis

Oxygen consumption rates (OCR) were measured using Seahorse XF96 analyzer. Briefly, 40,000 HUVECs were plated onto XF96 plates and incubated overnight at 37°C/5% CO₂. Next day, the media was replaced with XF assay media (DMEM, 1 g/L glucose, 2 mM glutamate, 1 mM pyruvate, pH 7.4). NaHS (0.1 mM) and/or NMN (0.5 mM) were added at the start of the experiment. OCR measurements were made approximately every 8 min under basal conditions, and after the addition of oligomycin (1 μ M). Experiments were replicated in six wells and averaged for each experimental condition.

Immunofluorescence

Freshly isolated whole quadriceps and gastrocnemius muscle samples were mounted in O.C.T. compound, placed in an isopentane bath and slowly cooled in liquid nitrogen. Transverse sections at 20 μ m-thickness were sectioned on a cryostat. The sections were fixed in pre-cooled acetone (-20°C) for 10 min. In case of cells, 4% paraformaldehyde in TBS (50 mM Tris-HCl, 150 mM NaCl, pH7.5) was used for fixation. The slides were washed with TBS twice and the tissues/cells were permeabilized by incubating with TBST (TBS + 0.1% Triton-X) for 10 min at room temperature. The slides were washed with TBS twice, blocked with BlockAid blocking solution for 1 h at room temperature, and then incubated with primary antibodies diluted in blocking buffer (1:100) overnight at 4°C. Next day, slides were washed with PBS and incubated with secondary antibodies (1:500 dilution) for 2 h at room temperature. Slides were washed again with TBS and mounted with mounting medium. Images were acquired using a confocal fluorescence microscope (Nikon A1). Muscle cross-sections were immunostained with anti-CD31 and anti-laminin antibodies to visualize capillaries and basal lamina surrounding the fibers, respectively. We restricted our examination to the mid-portion of the muscles because of its high capillary density and well-known adaptations to exercise (Chinsomboon et al., 2009). Quantification of capillaries and capillary density were performed using Fiji software. TUNEL staining was performed in muscle sections using TUNEL assay kit as per manufacturer's protocol.

Hematoxylin and eosin (H&E) staining

After fixation of frozen sections, samples were stained with 0.1% Hematoxylin for 10 min, rinsed with dH₂O, stained with Scott's blue solution for 1 min and then washed with dH₂O. The sections were then dipped in Eosin for 3 min, dehydrated through alcohol and cleared in xylene. The slides were mounted with DPX and imaged using Aperio XT Slide Scanner.

RNA analysis

Total mRNA was isolated from cells and tissues using TRIzol. cDNAs were synthesized from 1 µg of total RNA using iScript Reverse Transcription Supermix. qPCR was performed with LightCycler 48 SYBR Green I Mastermix using the LightCycler 480 System according to the manufacturer's instructions. Relative mRNA expression levels were calculated using the $\Delta\Delta C_t$ method. The forward and reverse primer sequences used in qPCR amplification reactions are displayed in [Table S2](#).

Western

SDS-PAGE and western blot analysis was performed according to standard procedures and detected with the ECL detection kit. Quantification of band intensities by densitometry was carried out using Fiji software.

QUANTIFICATION AND STATISTICAL ANALYSIS

Data are presented as means \pm SEM. Statistical significance was performed using Student's t test, one-way or two-way ANOVA with Bonferroni's Multiple Comparisons Test. Statistical test was performed using GraphPad Prism software. P values of less than 0.05 were considered statistically significant.

Supplemental Figures

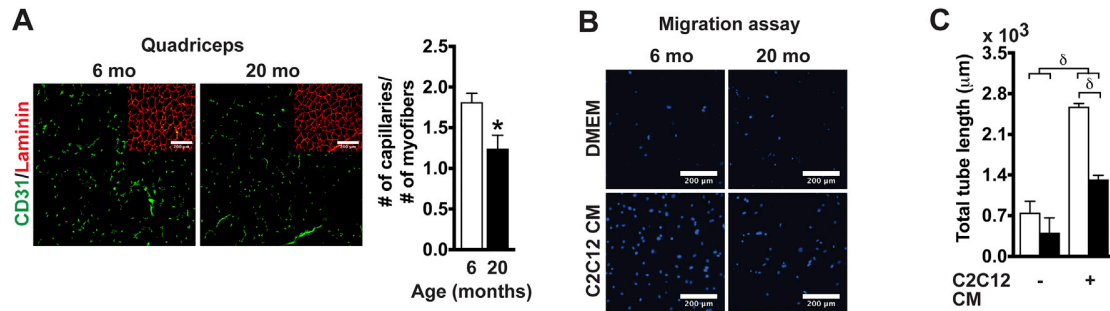


Figure S1. Aging Is Associated with Decreased Muscle Angiogenesis and Endurance, Related to Figure 1

(A) Images of quadriceps sections (@20X) from 6 and 20-month old mice showing CD31 and laminin staining. Quantification of capillary/myofiber ratio ($n = 5$).

(B) DAPI staining images of migrated MLECs.

(C) Tube length of capillary networks formed by MLECs ($n = 8$).

Data are expressed as mean \pm SEM. * $p < 0.05$, $^{\delta}p < 0.00005$ by Student's t test (A) or two-way ANOVA with Bonferroni's corrections (C).

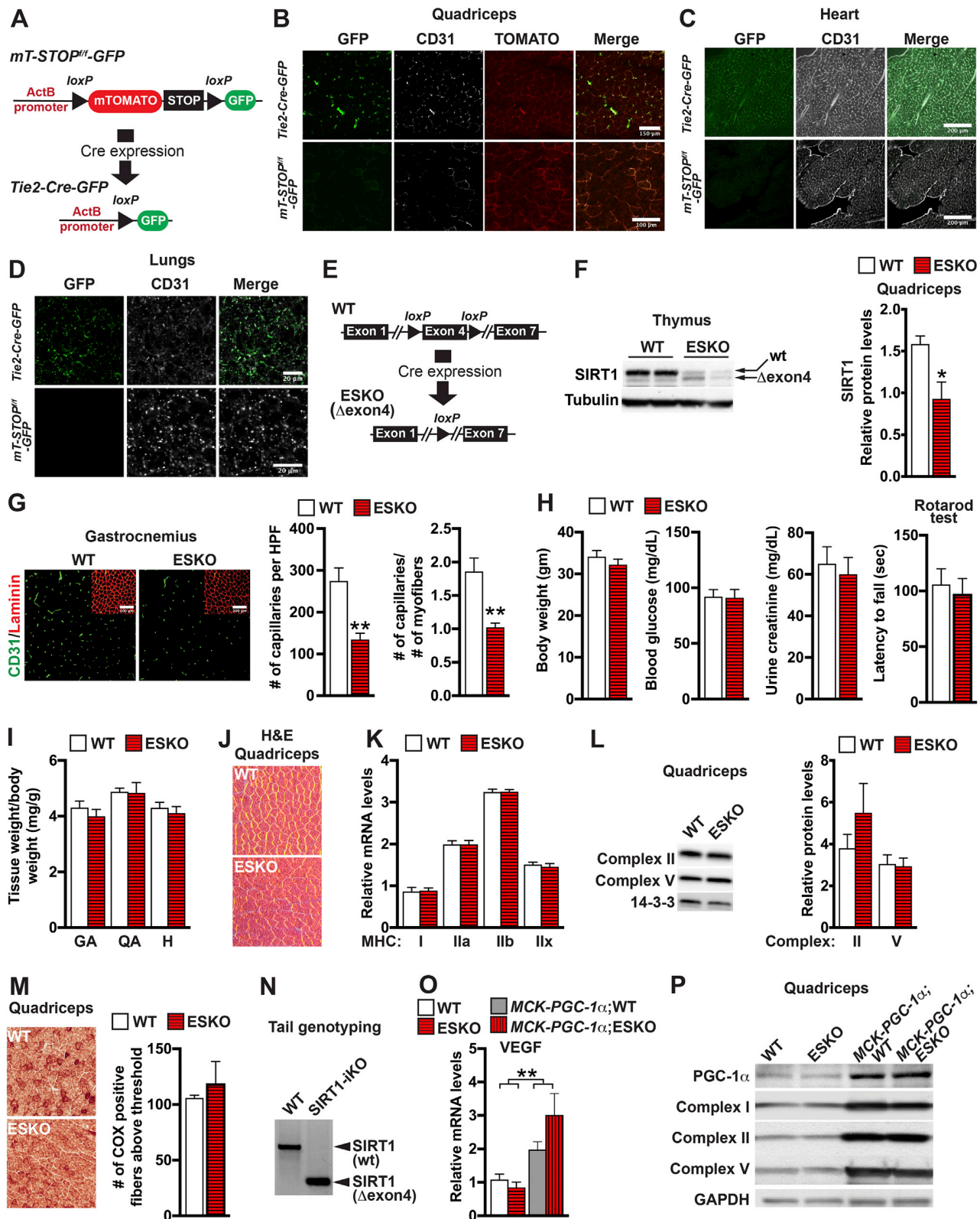


Figure S2. Endothelial SIRT1 Deletion Mimics the Effect of Aging on Capillary Density and Endurance, Related to Figure 2

(A) Strategy to generate EC-specific GFP reporter mouse (*Tie2-Cre-GFP*). *mT-STOP^{fl}-GFP* mouse expresses membrane-targeted tandem dimer Tomato (TOMATO) and when crossed to *Tie2-Cre* mouse (*Tie2-Cre-GFP*) expresses green fluorescent protein (GFP).

(B–D) Images of quadriceps (B), heart (C), and lung (D) sections (@40X) immunostained using GFP and CD31 antibodies, showing the expression of EC-specific GFP.

(E) Strategy to generate EC-specific SIRT1 knockout mouse (ESKO) by crossing a transgenic mouse that expresses Cre protein under the direction of EC-specific *Tie2* promoter (*Tie2-Cre*) and a mouse containing *loxP* sites flanking exon 4 (catalytic domain) of SIRT1 (*SIRT1^{fl/fl}* or WT).

(F) SIRT1 protein abundance in thymic tissue from WT and ESKO mice, in which the exon 4-excised SIRT1 band (Δ exon4) runs slightly below the wild-type (wt) SIRT1 band. Relative SIRT1 levels in the quadriceps from WT and ESKO mice for the western blot shown in Figure 2B (n = 3).

(G) Images of capillaries (CD31) and muscle stroma (laminin) in gastrocnemius sections (@20X). Number of capillaries and capillary/myofiber ratio (6-month old, n = 8).

(H) Body weights, fasting blood glucose levels, urine creatinine levels and rotarod performance showing time of latency to fall (6-month old, n = 7).

(I) Gastrocnemius (GA), quadriceps (QA) and heart (H) tissue weights normalized to body weights (6-month old, n = 7).

(J) H&E staining images of quadriceps from 6-month old WT and ESKO mice.

(K) Relative mRNA levels of myosin heavy chains I, IIA, IIB and IIX in gastrocnemius (6-month old, n = 10).

(L) Mitochondrial protein complexes II and V levels and relative. 14-3-3 as a loading control (6-month old, n = 4).

(M) COX staining images of quadriceps. Number of COX-positive fibers above a set threshold (6-month old, n = 4).

(N) PCR analysis of genomic DNA isolated from tails of WT and SIRT1-iKO mice showing the excision of SIRT1. SIRT1-iKO mouse expresses floxed allele of exon 4 (catalytic domain) of SIRT1 and ubiquitous CAG promoter driven Cre-esr1 fusion protein. Cre protein was activated upon treatment with 4-hydroxytamoxifen, resulting in deletion of exon 4. Full-length wild-type SIRT1 (wt) is evident in WT mice, while a smaller band corresponds to a loss of SIRT1 exon 4 (Δ exon4).

(O) Relative mRNA levels of VEGF in quadriceps (4-month old, n = 5).

(P) PGC-1 α , NDUFB5 (Complex I), SDH8 (Complex II) and ATP5a (Complex V) protein levels in quadriceps. GAPDH as a loading control (4-month old).

Data are expressed as mean \pm SEM. *p < 0.05, [§]p < 0.00005 by Student's t test (F and G) or two-way ANOVA with Bonferroni's corrections (O).

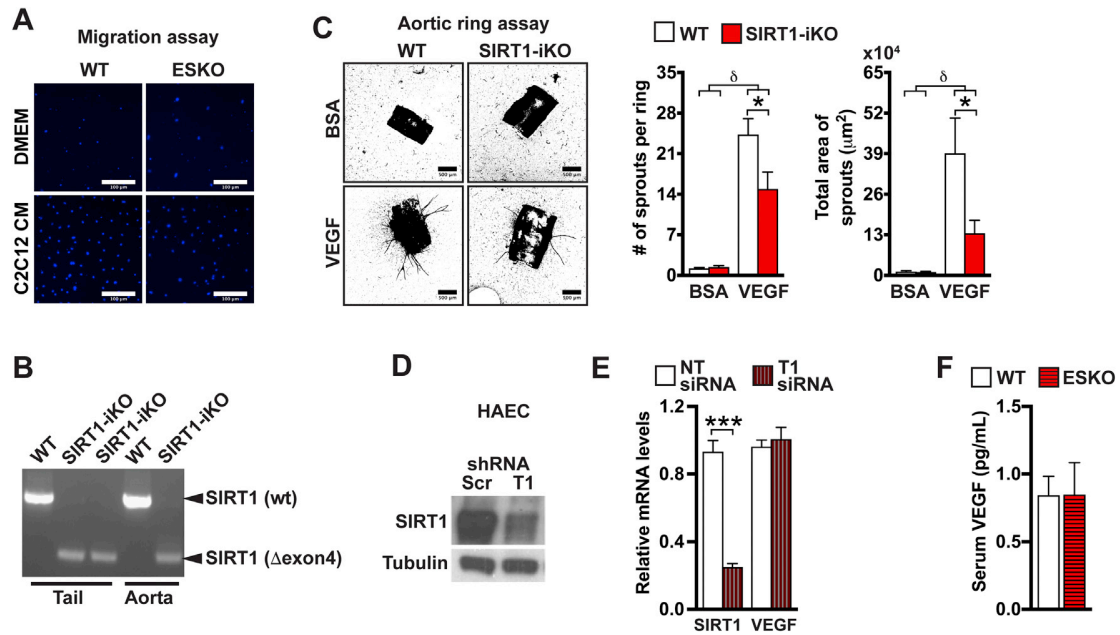


Figure S3. SIRT1 Is Required for Angiogenesis *In Vitro*, Related to Figure 3

(A) DAPI staining images of migrated MLECs.

(B) PCR analysis of genomic DNA isolated from tails and aorta showing the excision of SIRT1.

(C) Images, number and total area of microvessel sprouts in VEGF stimulated aortic rings ($n = 8$).

(D) SIRT1 protein levels in HAECs infected with lentivirus expressing scrambled (Scr) or SIRT1 (T1) shRNAs.

(E) Relative SIRT1 and VEGF mRNA levels in HUVECs transduced with non-targeting (NT) or SIRT1 (T1) siRNAs ($n = 3$).

(F) VEGF protein levels in serum collected from 6-month old WT and ESKO mice ($n = 5$).

Data are expressed as mean \pm SEM. * $p < 0.05$, $^{\delta}p < 0.00005$ by Student's t test (E) or two-way ANOVA with Bonferroni's corrections (C).

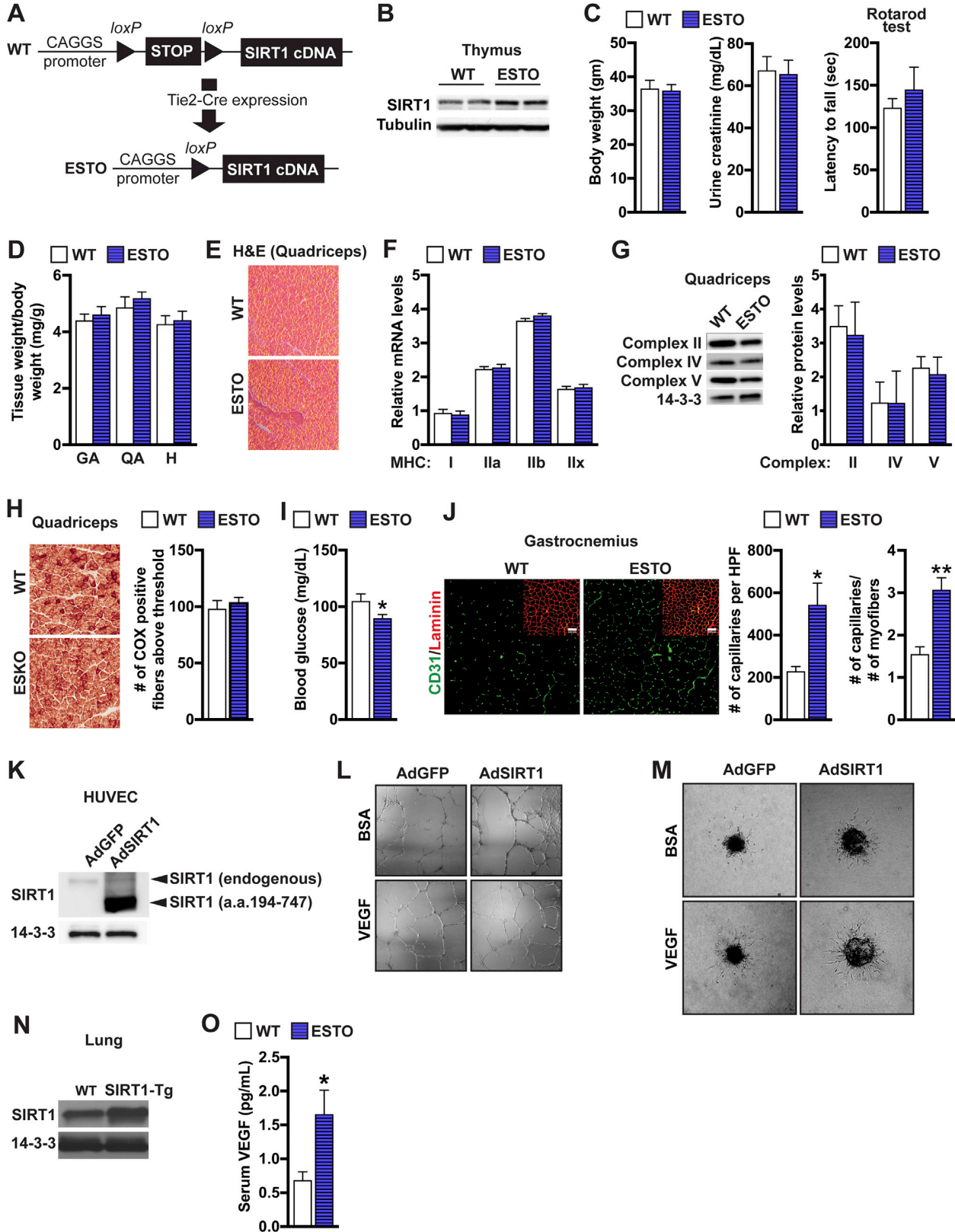


Figure S4. Endothelial SIRT1 Increases Capillary Density and Exercise Capacity, Related to Figure 4

- (A) Strategy to generate EC-specific SIRT1 overexpression mouse (ESTO) by crossing *Tie2-Cre* mouse and *SIRT1^{STOP}* (WT) mouse. *SIRT1^{STOP}* mouse expresses a transgene in which SIRT1 has been cloned downstream of a constitutive CAGGS promoter followed by a transcriptional *loxP-STOP-loxP* cassette.
- (B) SIRT1 protein abundance in thymic tissue from 6-month old WT and ESTO mice. Tubulin serves as a loading control.
- (C) Body weights, urine creatinine, and rotarod performance showing time of latency to fall (6-month old, n = 7).
- (D) Gastrocnemius (GA), quadriceps (QA) and heart (H) tissue weight normalized to body weight (6-month old, n = 7).
- (E) H&E staining images of quadriceps from 6-month old WT and ESTO mice.
- (F) Relative mRNA levels of myosin heavy chains I, IIA, IIB and IIX in gastrocnemius (6-month old, n = 10).
- (G) Mitochondrial protein complexes II, IV and V abundance in quadriceps. 14-3-3 as loading control. Quantifications of complexes are shown (6-month old, n = 4).
- (H) COX staining images of quadriceps. Number of COX positive fibers above a set threshold (6-month old, n = 4).
- (I) Fasting blood glucose levels (6-month old, n = 7).
- (J) Images of capillaries (CD31) and muscle stroma (laminin, inset) in gastrocnemius sections (@20X). Number of capillaries and capillary/myofiber ratio (6-month old, n = 8).
- (K) SIRT1 protein level in HUVECs infected with adenoviruses expressing GFP or SIRT1 (aa194-747). The overexpressed SIRT1 runs slightly below the endogenous SIRT1 in adeno-SIRT1 infected cells. 14-3-3 as a loading control.
- (L) Images of the tube networks formed by VEGF stimulated HUVECs infected with AdGFP or AdSIRT1.
- (M) Images of the spheroids from Ad-GFP or Ad-SIRT1 transduced HUVECs stimulated with VEGF.
- (N) SIRT1 protein levels in lungs. 14-3-3 as a loading control.
- (O) VEGF protein levels in serum (6-month old, n = 5).
- Data are expressed as mean \pm SEM. *p < 0.05, **p < 0.005 by Student's t test (I, J and O).

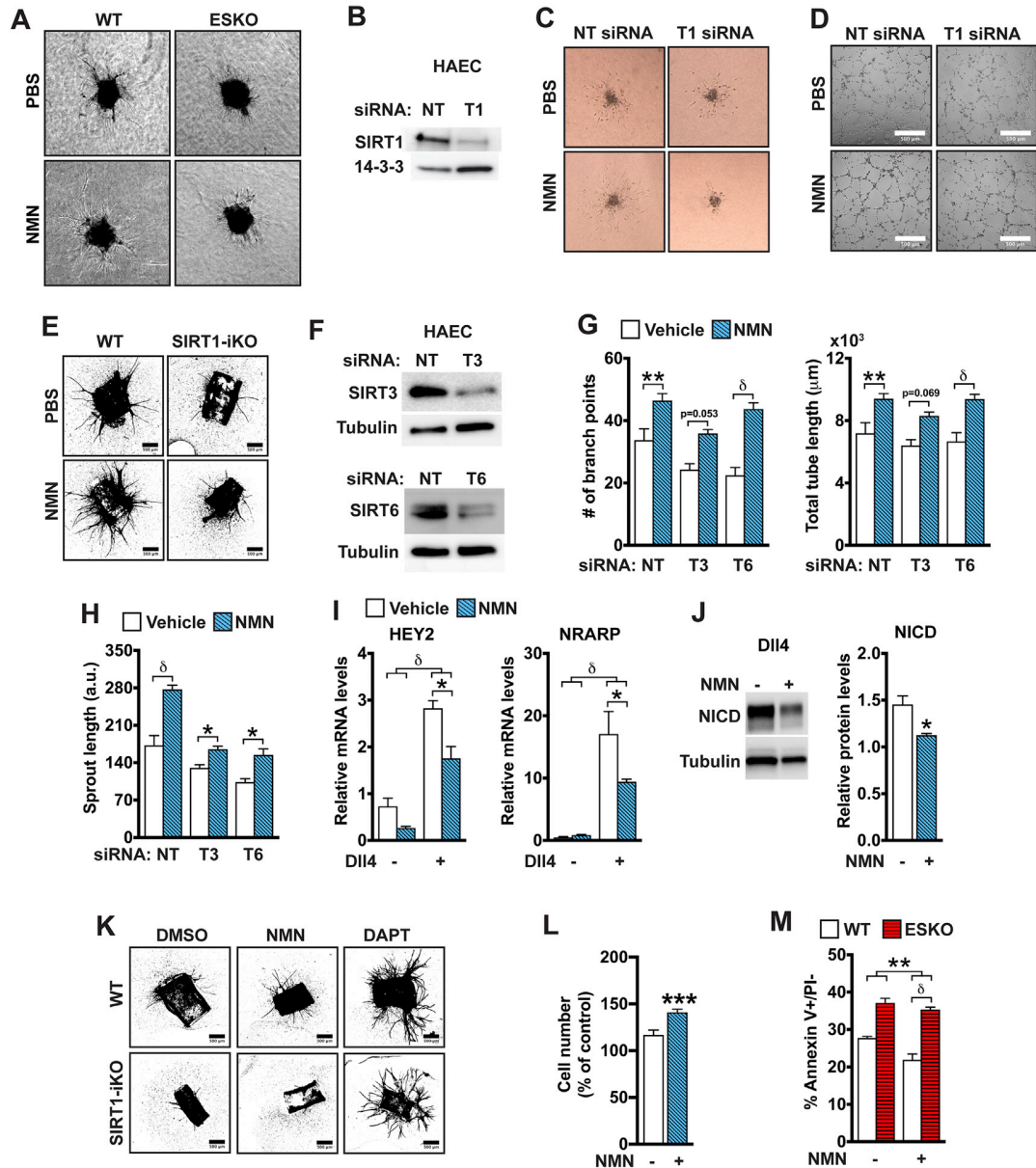


Figure S5. Endothelial NAD⁺ Sensitizes ECs to VEGF by Suppressing Notch, Related to Figure 5

(A) Images of the spheroids from C2C12 CM stimulated MLECs.

(B) SIRT1 protein levels in HAECs transfected with non-targeting (NT) or SIRT1 (T1) siRNAs. 14-3-3 as loading control.

(C) Images of the spheroids from VEGF stimulated HAECs transfected with NT or T1 siRNAs.

(D) Images, number of branch points and length of tube networks formed by HAECs transfected with NT or T1 siRNAs and stimulated with VEGF (n = 12).

(E) Images of microvessel sprouts in aortic rings stimulated VEGF.

(F) SIRT3 and SIRT6 protein levels in HAECs transfected with NT, SIRT3 (T3) or SIRT6 (T6) siRNAs. Tubulin serves as a loading control.

(G) Number of tube branch points and length of the tube networks formed by HAECs transfected with NT, T3 or T6 siRNAs under VEGF stimulation (n = 10-12).

(H) Sprout length of the spheroids from HAECs transfected with NT, T3 or T6 siRNAs and stimulated with VEGF (n = 8).

(I) Relative mRNA levels of Notch target genes (HEY2 and NRARP) in HAECs stimulated with DII4 for 1 hr (n = 3).

(J) NICD protein in HAECs stimulated with DII4 for 5 hr. Relative abundance of NICD protein (n = 3).

(K) Images of microvessel sprouts in aortic rings stimulated with VEGF.

(L) Relative HUVEC number after incubation with \pm NMN for 48 h and measured using flow cytometry (n = 12).

(M) Number of apoptotic MLECs (Annexin V+/PI-), serum-starved overnight \pm NMN and analyzed using flow cytometry (n = 12).

Data are expressed as mean \pm SEM. *p < 0.05, **p < 0.005, ***p < 0.0005, δ p < 0.00005 by Student's t test (J and L), one-way (G and H) or two-way (I and M) ANOVA with Bonferroni's corrections.

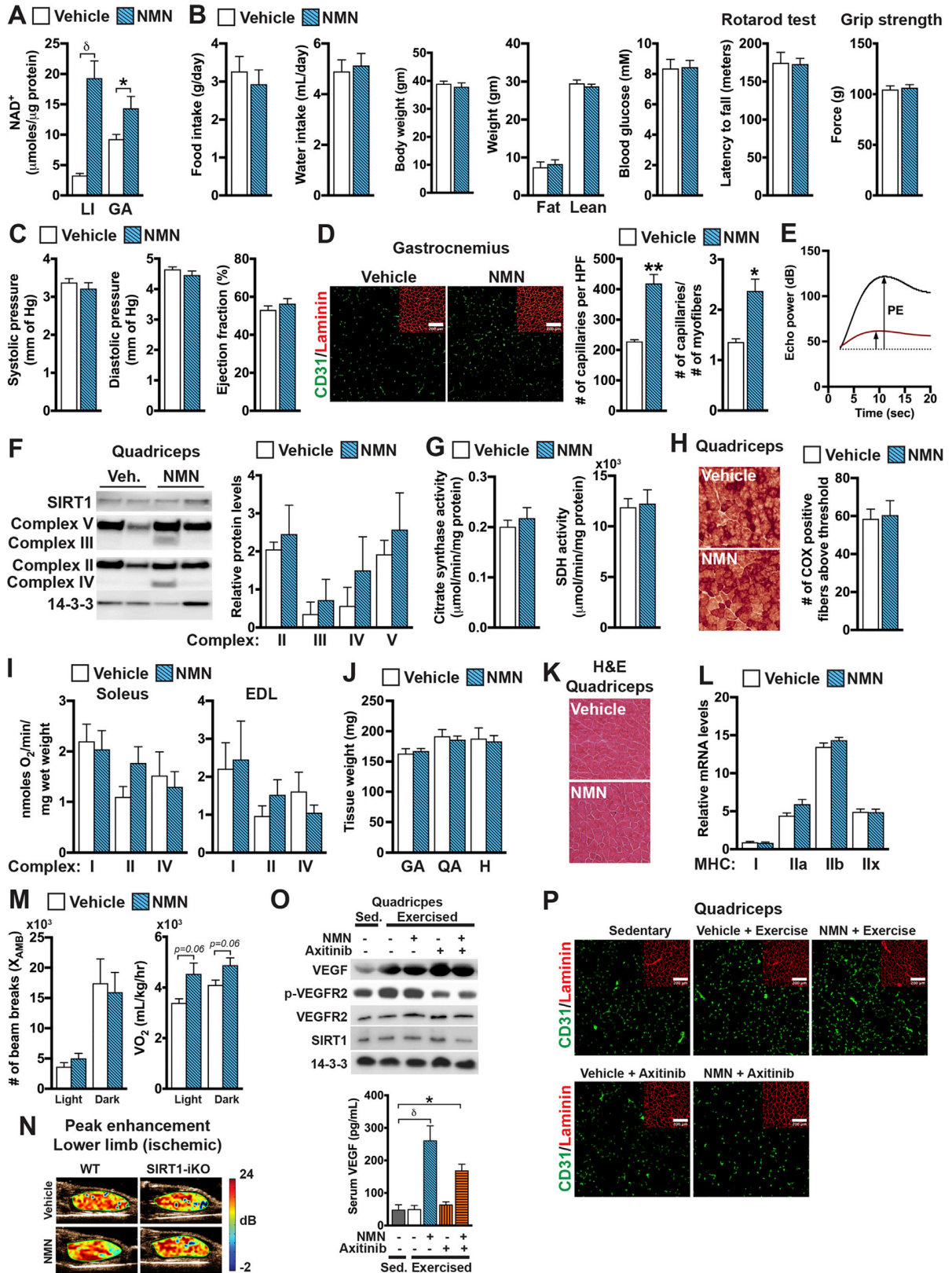


Figure S6. NAD Repletion Restores the Microvasculature and Exercise Capacity of Old Mice, Related to Figure 6

- (A) NAD⁺ levels in the liver (L) and gastrocnemius (GA) tissues from vehicle and NMN-treated mice (18-month old) normalized to the total protein content (n = 12-14).
- (B) Food intake, water consumption, body weights, lean mass, fat mass, fasting blood glucose, rotarod performance and grip strength (20-month old, n = 10).
- (C) Systolic pressure, diastolic pressure, and ejection fraction measured using echocardiography (20-month old, n = 10).
- (D) Images of capillaries (CD31) and muscle stroma (laminin) in gastrocnemius sections (@20X). Number of capillaries and capillary/myofiber ratio (20-month old, n = 8).
- (E) Representation of peak enhancement (PE) measured using contrast-enhanced ultrasound.
- (F) SIRT1 and mitochondrial complexes II, III, IV and V protein in quadriceps. 14-3-3 as loading control. Relative abundance of mitochondrial complexes (20-month old, n = 4).
- (G) Citrate synthase and succinate dehydrogenase (SDH) activities in quadriceps (20-month old, n = 10).
- (H) COX staining images of quadriceps. Number of COX positive fibers above a set threshold (20-month old, n = 4).
- (I) Oxygen consumption rates mediated through mitochondrial complexes I, II and IV in soleus and EDL permeabilized muscle fibers measured using a Clark electrode system (20-month old, n = 10).
- (J) Gastrocnemius (GA), quadriceps (QA) and heart (H) tissue weights (20-month old, n = 13).
- (K) H&E staining images of quadriceps from 20-month old vehicle and NMN-treated mice.
- (L) Relative mRNA levels of myosin heavy chains I, IIA, IIB and IIX in gastrocnemius (20-month old, n = 13).
- (M) Locomotor activity (Xamb – successive beam breaks in the x axis) and oxygen consumption rates (VO₂) measured using Oxymax-CLAMS system (20-month old, n = 6).
- (N) Peak enhancement-mode ultrasound images of the ischemic hindlimbs of vehicle and NMN-treated mice measured 20 days post-femoral ligation.
- (O) VEGF, VEGFR2, phospho-VEGFR2 and SIRT1 protein levels in quadriceps from 5-month old WT mice that were kept sedentary or exercised ± NMN, ± axitinib. 14-3-3 as loading control. Serum VEGF measured by ELISA (n = 5).
- (P) Images of capillaries (CD31) and muscle stroma (laminin) in quadriceps sections (@20X) from 5-month old WT mice that were kept sedentary or exercised ± NMN, ± axitinib.
- Data are expressed as mean ± SEM. *p < 0.05, **p < 0.005, ³p < 0.00005 by Student's t test (A, D and M) or one-way ANOVA with Bonferroni's corrections (O).

